Global cobalt resources, production and future sources of supply

Carolin Kresse, Gus Gunn, Eva Petavratzi
British Geological Survey, UK

Abstract. Cobalt is a critical metal with numerous applications in new and green technologies. Global demand, particularly for use in lithium-ion batteries, is forecast to increase rapidly. Consequently, to ensure security of cobalt supply, it is important to diversify the cobalt supply base, to expand our knowledge of its occurrence in known mineral deposits and to identify new resources. Cobalt may be enriched in a variety of geological settings. The most important deposit types with cobalt resource potential are sediment-hosted stratabound copper deposits, nickel-cobalt laterite deposits and magmatic nickel-copper deposits. About 60 per cent of mined cobalt is a by-product of copper mining, mainly in the Central African Copperbelt. The remainder is derived from several other deposit types, although less than two per cent is from primary cobalt producers such as Bou Azzer in Morocco. Potential new onshore sources of cobalt are widespread in the United States, Canada, Australia, the DRC, Zambia and Madagascar, and offshore in deep-sea manganese nodules and cobalt-rich ferromanganese crusts.

1 Introduction

The European Union (EC 2017) classifies cobalt as a critical metal. More than half of global mine production of cobalt is from the DRC, a country noted for its political and economic instability and the association of mining with armed conflict and the use of child labour. Cobalt is widely used in a range of hi-tech applications, most notably in decarbonising the transport sector. Cobalt is an important constituent of the cathodes in most lithium-ion batteries used in electric vehicles (EV). The recent growth in the global EV market and its forecast continued expansion will inevitably lead to increased demand for raw materials such as cobalt (IEA 2018). Consequently, in order to ensure future security of supply, it is becoming increasingly important to diversify the global supply base for cobalt. Improving our deposit models for cobalt enrichment in the crust will facilitate the identification of new resources.

2 Deposit types

Cobalt is found in economic concentrations in three main deposit types: sediment-hosted stratabound copper deposits (SHSC); nickel-cobalt laterite deposits; and magmatic nickel-copper (-cobalt±PGE) sulfide deposits (Naldrett 2004; Mudd et al. 2013). The largest cobalt-producing region is the Central African Copperbelt (CACB) in the DRC and Zambia, with some large deposits also known in Australia, Russia, Cuba, New Caledonia and Canada (Fig. 1).

SHSC deposits (Taylor et al. 2013) are not only the world's second largest source of copper, but are also the most important source of cobalt accounting for approximately 60 per cent of global cobalt mine production (Brown et al. 2019).

Nickel lateritesassociated with ultramafic rocks may also contain appreciable concentrations of cobalt between 0.025 and 0.18% (Berger et al. 2011; Slack et al. 2017). The Murrin Murrin deposit in Western Australia (Gaudin et al. 2005) and the Goro deposit in New Caledonia (Wells et al. 2009) are examples of some of the world's many large nickel-cobalt laterite deposits. The manganiferous Nkamouna cobalt-nickel deposit in Cameroon is one of the few in which cobalt would be the principal economic metal to be mined (Lambiv Dzemua and Gleeson 2012). Ore reserves in this and the nearby Mada deposit were 68.1 million tonnes grading at least 0.26% Co (SRK 2011), representing possibly one of the largest undeveloped cobalt reserves in the world.

Magmatic nickel-copper (-cobalt±PGE) deposits comprise: (1) magmatic sulfide deposits; and (2) magmatic PGE deposits in layered intrusions. Magmatic sulfide deposits account for about 60 per cent of global nickel production (Naldrett 2004) with cobalt contents of the iron-nickel-copper sulfide ores in some deposits reaching 500–1000 ppm (Mudd et al. 2013). Globally, two prominent nickel-copperdistricts exist each containing more than 20 million tonnes of nickel metal: Sudbury, Ontario, Canada and Noril'sk-Talnakh, Russia (Schulz et al. 2014). Naldrett (2004) reported an average Co grade of 0.038% in the Sudbury ores. Ore reserves in the Noril'sk-Talnakh deposits amount to 215 million tonnes grading 0.016% Co (Noril'sk Nickel 2014).

The most important magmatic PGE deposits in layered intrusions are located in the Bushveld Complex in South Africa, the Great Dyke in Zimbabwe and in the Stillwater Complex in the United States. Hitzmann et al. (2017) reported Co grades of 0.03% in Bushveld ores, and appreciable amounts of cobalt (7–18 wt%) in manganese-cobalt-nickel-copper-oxides and hydroxides at the Great Dyke (Oberthür et al. 2013).

Cobalt may also be concentrated in a variety of other geological settings and deposit types including: cobalt-copper-gold deposits in metasedimentary rocks; cobalt-rich vein deposits; iron-oxide-copper-gold deposits (IOCG); volcanogenic massive sulfide deposits; black shale hosted nickel-copper-zinc-cobalt deposits etc.

Significant concentrations of cobalt occur in iron-manganese-rich nodules and cobalt-rich crusts, although to date no cobalt has been extracted from these. Iron-manganese-rich nodules, typically 1–5 cm in size, found

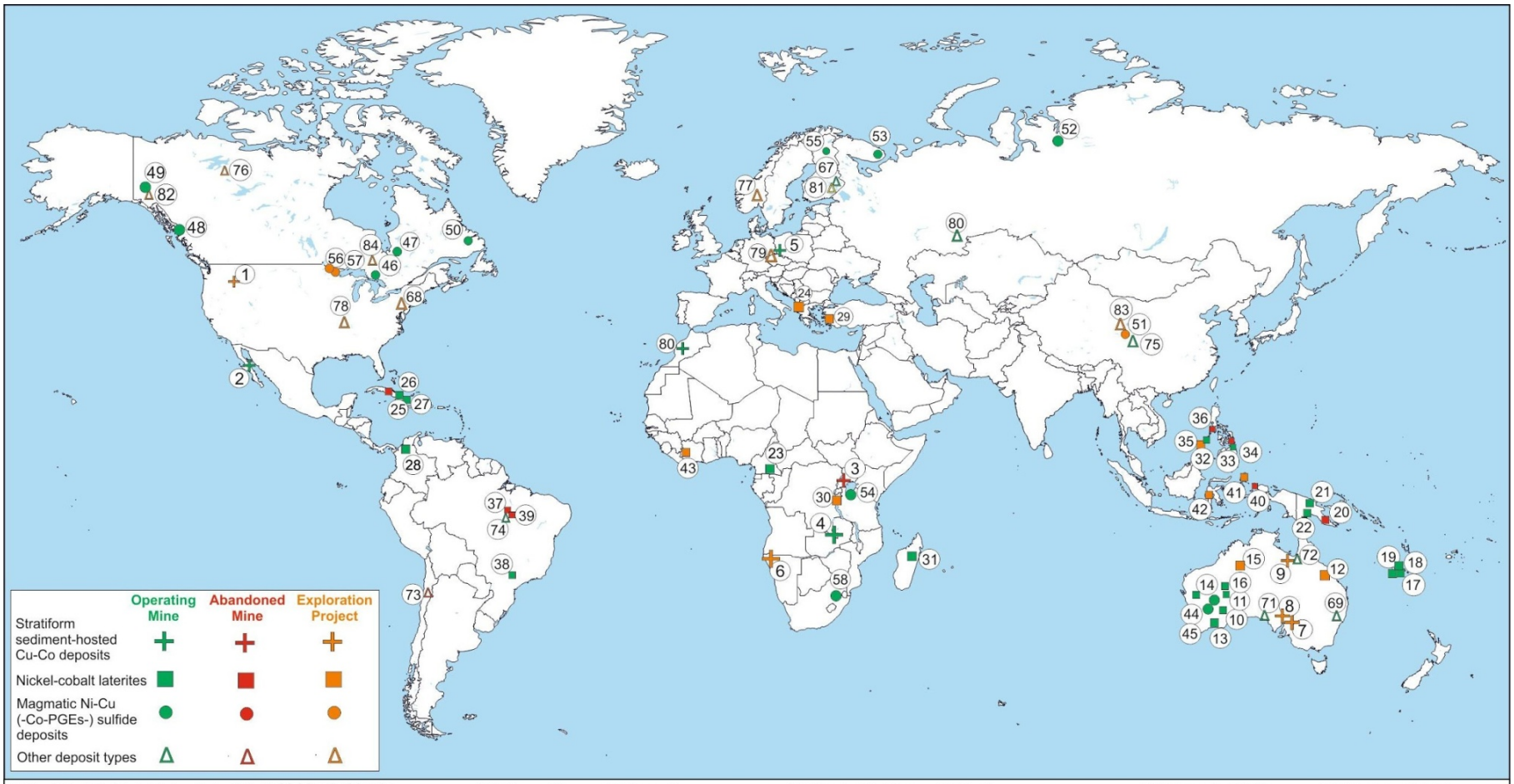

1 Blackbird district, Idaho Cobalt Belt
2 Boleo
3 Kilembe
4 Central African Copper Belt
5 European Kupferschiefer (Lubin Mine district)
6 Opuwo Cobalt Project
7 Thackaringa Cobalt, Broken Hill
8 Emmie Bluff and Windabout
9 Mount Isa
10 Kalgoorlie
11 Murrin Murrin
12 Marlborough Cobalt
13 Ravensthorpe
14 Weld Range
15 Wingellina Nickel-Cobalt
16 Cawse
17 Goro
18 Nakety
19 Thio
20 Mambare
21 Ramu
22 Wowo Gap
23 Nkamouna
24 Bitincke
25 Moa
26 Punta Gorda
27 Nicaro
28 Cerro Matosa
29 Caldag
30 Musongati
31 Ambatovy
32 Coral Bay
33 Taganito
34 Nonoc
35 Ipilan
36 Mindoro
37 Jacaré
38 Niquelandia
39 Vermelho
40 Gag Island
41 Halmahera/Weda Bay
42 La Sampala
43 Tiuba-Biankouma
44 Kambalda Dome
45 Mt. Keith
46 Sudbury
47 Dumont
48 Turnagain
49 Wellgreen
50 Voisey's Bay
51 Jinchuan
52 Norilsk-Talnakh
53 Pechenga
54 Kabanga
55 Kevitsa
56 Nokomis
57 Northmet
58 Nkomati
59 Clarion-Clipperton Zone
60 Cook Islands EEZ
61 Pioneer
62 Pacific prime crust zone
63 Nameless
64 Unicorn
65 Maderia-Tore Rise (MTR)
66 Afanasiy-Nikitin
67 Talvivaara
68 Cornwall/Morgantown
69 Mount Elliott
70 Magnitogorsk
71 Olympic Dam
72 Ernest Henry
73 Candelaria
74 Sossego
75 Lala (Lalachang)
76 NICO
77 Modum district
78 Mine La Motte/ Fredericktown
79 Erzgebirge
80 Bou Azzer
81 Outokumpu
82 Windy Craggy
83 Deerni
84 Cobalt-Gowganda Dist.
85 Gaiskoye
86 Kilembe and Bujagali

Figure 1: Selected cobalt deposits worldwide (Co content > 0.05 million tonnes*) (operating, abandoned, exploration project). *Estimated Co contents of exploration projects may be lower than 0.05 million tonnes. Other deposits include: Black shale-hosted Ni-Cu-Zn-Co, Fe-Cu-Co skarn and replacement deposits, Iron oxide Cu-Au (-Ag-U-REE-Co-Ni), Metasedimentary rock-hosted Co-Cu-Au, MVT sulfide deposits, Cobalt-rich vein deposits, VMS sulfide deposits (Data from Mudd et al. 2013; Slack et al. 2017; company reports, websites and other publications)

at water depths of 4.5–6 km, may be strongly enriched relative to the Earth's crust in nickel, copper and cobalt (Hein et al. 2013).

The largest known occurrences are located in the eastern equatorial Pacific Ocean between the Clarion and Clipperton fracture zones (CCZ), in the Cook Islands Exclusive Economic Zone (EEZ), in the Penrhyn-Samoa Basin, in the Peru Basin, and in the Pioneer area of the central Indian Ocean (Hein et al. 2013). Cobalt grades in these nodules seldom exceed 2000 ppm, but, given the high nodule densities and the vast extent of these fields, the resource potential is very large.

Ferromanganese crusts are thickest and most metal-enriched on the flanks of seamounts at water depths of 800–2500 m. They are most abundant in the north-west Pacific Ocean. The Prime Crust Zone (PCZ) in the central and western equatorial Pacific is currently of greatest economic interest (Hein et al. 2013). The cobalt content of these crusts can be up to 2 wt%, but generally averages between 0.30 and 0.67 wt% (Hein et al. 2013).

3 World resources and reserves

The terrestrial cobalt resource is about 25 million tonnes (USGS 2019). The largest share of global resources, about 15 million tonnes, is located in the CACB in the DRC and Zambia (Hitzmann et al. 2017). In the CACB most economic cobalt resources occur in the Congo Copperbelt (CCB) and the Western portion of the Zambian Copperbelt (ZCB). The Tilwezembe structure (in the CCB) contains some of the most cobalt-rich deposits; several have grades sufficient for primary cobalt production, e.g. Kisanfu (1.1% Co) (Hitzmann et al. 2017).

Various estimates of cobalt resources in iron-manganese nodules and crusts on the seafloor should be considered as indicative geological endowments and are not mineral resources in the strict sense. USGS (2019) reports more than 120 million tonnes of cobalt resources in the Atlantic, Indian and Pacific oceans. Hein and Koschinsky (2014) reported that the CCZ alone contains 21 billion tonnes of nodules with a cobalt content of 40 million tonnes. Based on a mean cobalt content of 0.66%, the estimated total cobalt resource in the PCZ is about 50 million tonnes (Hein et al. 2013).

Global cobalt reserves amount to 6.9 million tonnes (USGS 2019). The DRC has the largest share of the reserves with about 49.5 per cent (3,400,000 tonnes), followed by Australia (17.5per cent), Cuba (7.3 per cent) and the Philippines (4.1 per cent) (Fig.2).

4 World production

More than half of global mine production of cobalt comes from the DRC, which produces about59 per cent of the total. Other significant producers include New Caledonia, China, Canada, Australia, Cuba, Zambia and Morocco (Brown et al. 2019). Almost all cobalt is produced as a by-product. In the DRC and Zambia, it is a by-product of the extraction of copper from SHSC deposits, while elsewhere most cobalt production is a by-product of nickel mining. For example, in Cuba, New Caledonia and Madagascar the cobalt is derived from nickel-cobalt laterite deposits. Elsewhere, for example in Canada and Russia and China, most cobalt is extracted from magmatic nickel sulfide deposits. In Australia and Brazil, cobalt is derived as a by-product of mining both laterite and magmatic sulfide deposits. At only one operating mine, Bou Azzer in Morocco, is cobalt extracted as the main economic product (Bouabdellah et al, 2016). In contrast to mine production, refined cobalt production (both metal and chemicals) is dominated by China, which produces about58 per cent of the world total, with other substantive cobalt refining capacity in Finland (10per cent) and Zambia (2.1 per cent). China sources more than 90 per cent of its feed material for the production of refined cobalt from the DRC, with the DRC itself producing only 0.2 per cent of the world's refined cobalt (Brown et al. 2019).

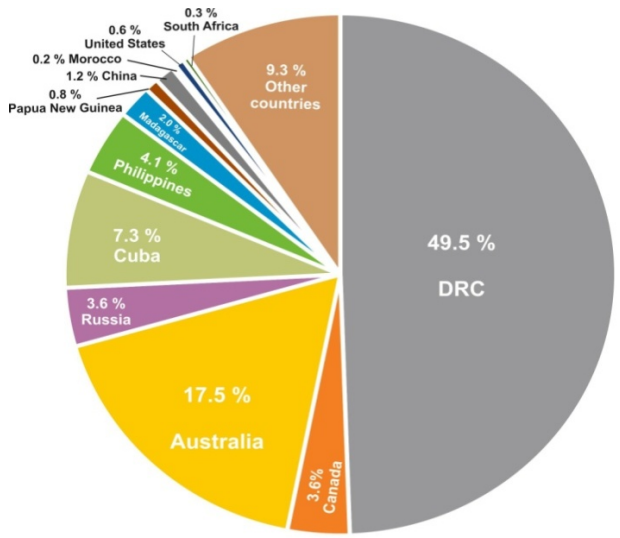

Figure 2. World cobalt reserves by country (USGS Mineral Commodity Summary 2019).

5 Expanding the resource base

Until recently, the small size of the global market for cobalt (about 100,000 tonnes contained metal per annum) and its price have meant that it has not been economic to mine cobalt alone. However, with rapidly growing demand and a concomitant rise in the price of cobalt, there has been significant growth in exploration for new cobalt resources. Numerous targets are being investigated worldwide. For example, Battery Mineral Resources is prospecting in the Ontario Cobalt Belt, where numerous projects demonstrate high-grade cobalt values ranging from 1.5% to 21%, and mineral resources of 72,000 tonnes grading 1.27% Co (Battery Mineral Resources 2018).Fortune Minerals Ltdplans to develop a mine at the NICO deposit in Canada, where mineral reserves total 33 million tonnes, containing c. 37200 tonnes of cobalt in open pit and 600 tonnes underground (Fortune Minerals Ltd 2014). The Thackaringa Cobalt Project in Australia has indicated resources of 72 million tonnes at 852 ppm Co for 61.5 kilo tonnes contained cobalt (Cobalt Blue Holdings 2018). At the Opuwo Cobalt Project in Namibia a mineral resource of 112.4 million

tonnes grading 0.11% Co has been identified (Celsius Resources Ltd 2018).

Increasing demand for cobalt is also driving exploration for new depositsin European countries, where only limiteddeposits are known. In 2017 the EU launched a European Battery Alliance aimed at creating a competitive EV manufacturing sector throughout Europe (https://www.eba250.com/). A key objective of the Alliance is to evaluate the potential for resources of battery raw materials in the EU. Ores in the Kupferschiefer deposits in Poland, mined by KGHM Polska Miedz S.A., have average contents of 50–80 ppm Co (Pazik et al. 2016). Boreal Metals Corp. owns several projects in Scandinavia, focusing on new targetsin known mining districts, e.g. the Los Cobalt Mine, Sweden and the Modum project, Norway (Boreal Metals Corp. 2019).The Geological Survey of Finland has started a major programme to identify areas favourable for the occurrence of battery raw materials in Finland to ensure future supply in Europe (GTK 2018). Important Ni-Co laterites are found in the region stretching from Serbia through to Turkey, but many of them are still undeveloped. The current bulk Ni-Co production comes from Greece, accounting for about 1% of world production of Ni with other mines in Turkey, Albania, and Kosovo. The Mokra Gora deposit in Serbia is a potentially large but low-grade redeposited lateritic deposit, indicating a resource of more than 1 billion tonnes at 0.7% Ni and 0.05% Co. Newly advanced technologies regarding mineral processing could make the region more attractive for Ni and co-recovery of Co (Herrington et al., 2016).

Acknowledgements

The authors are grateful to BGS colleagues, Simon J. Kemp and Stefan Horn, for their reviews of this paper. The authors publish with the permission of the Executive Director, British Geological Survey (UKRI).

References

Battery Mineral Resources (2018) Investor Presentation, 20 pp https://www.batterymineralresources.com/site/assets/files/4814/investorpresentation_bmr_12_18.pdf.

Berger VI, et al. (2011) Ni-Co Laterite Deposits of the World—Database and Grade and Tonnage Models, USGS Open-File report, 26 pp.

Boreal Metals Corp. (2019) Corporate Presentation http://www.borealmetals.com/_resources/presentations/corporate-presentation.pdf.

Bouabdellah, M., Maacha, L., Levresse, G., Saddiqi, O., 2016, The BouAzzer Co–Ni–Fe–As (±Au±Ag) District of Central Anti-Atlas (Morocco): A Long-Lived Late Hercynian to Triassic Magmatic-Hydrothermal to Low-Sulphidation Epithermal System. In Mineral Deposits of North Africa (pp. 229-247). Springer, Cham.

Brown TJ, et al. (2019) World Mineral Production 2013-17. British Geological Survey, Keyworth, Nottingham.

Celsius Resources Ltd (2018) Building an Extensive Cobalt Resource in Namibia, Africa down under http://clients3.weblink.com.au/pdf/CLA/02015894.pdf.

Cobalt Blue Holdings (2018) Financial Report https://www.cobaltblueholdings.com/thackaringa-resource/.

EC, 2017. Critical Raw Materials Factsheets: Cobalt. https://publications.europa.eu/en/publication-detail/-/publication/7345e3e8-98fc-11e7-b92d-01aa75ed71a1/language-en.

Fortune Minerals Limited (2014) Technical Report on the Feasibility Study for the NICO Gold-Cobalt-Bismuth-Copper project Northwest Territories, Canada, 385 pp.

Gaudin A, et al. (2005) Clay mineralogy of the nickel laterite ore developed from serpentinised peridotites at Murrin Murrin, Western Australia, Aust J Earth Sci 52: 231–241.

Geological Survey of Finland (2018) Geofoorumi Stakeholder magazine http://verkkolehti.geofoorumi.fi/wp-content/uploads/sites/1/2019/01/geofoorumi_2_122018_naytto.pdf.

Hein JR, et al. (2013) Deep-ocean mineral deposits as a source of critical metals for high- and green-technology applications-Comparison with land-based resources. Ore Geol Rev 51:1–14.

Hein JR, Koschinsky A(2014) Deep-Ocean ferromanganese crusts and nodules. In Treatise on Geochemistry, Elsevier, Amsterdam, 2: 273–291.

Herrington R, et al. (2016) Bauxite and Nickel-Cobalt Lateritic Deposits of the Tethyan Belt. Econ Geol19:349-387.

Hitzman MW, Bookstrom AA, Slack JF, Zientek ML (2017) Cobalt—Styles of deposits and the search for primary deposits: USGS Open-File Report, 47 pp, https://doi.org/10.3133/ofr20171155.

IEA (2018) Global EV Outlook 2018. Towards cross-modal electrification. International Energy Agency.

Lambiv Dzemua G, Gleeson SA (2012) Petrography, mineralogy, and geochemistry of the Nkamouna serpentinite—Implications for the formation of the cobalt-manganese laterite deposit, southeast Cameroon. Econ Geol 107:25–41.

M2Cobalt (2017) Technical Report for the Bujagali and Kilembe Properties https://www.m2cobalt.com/images/pdf/Technical_Report_m2Cobalt.pdf.

Mudd GM, et al. (2013) Quantifying the recoverable resources of by-product metals-The case of cobalt, Ore Geol Rev 55:87–98.

Naldrett AJ (2004) Magmatic Sulfide Deposits: Geology, Geochemistry and Exploration, Berlin, Germany: Springer.

Norilsk Nickel (2014) Annual report https://www.companyreporting.com/sites/default/files/annual-report-index/norilsk-nickel-annual-report-2014.pdf.

Oberthür T, et al. (2013) The oxidized ores of the main sulphide zone, Great Dyke, Zimbabwe: Turning resources into minable reserves – mineralogy is the key, J South Afr Inst Min Metall 113:191-201.

Pazik PM, et al. (2016) World production and possible recovery of cobalt from the Kupferschiefer stratiform copper ore. In E3S Web of Conferences, EDP Sciences 8:01063.

Roberts S, Gunn G (2014) Cobalt. Critical Metals Handbook, pp 122-149.

Slack FJ, Kimball BE, Shedd KB (2017) Cobalt Chapter F of Critical Mineral Resources of the United States - Economic and Environmental Geology and Prospects for Future Supply.Professional paper 1802-F. USGS.

Schulz KJ, Woodruff LG, Nicholson SW, Seal II RR, Piatak NM, Chandler VW, Mars JL (2014) Occurrence model for magmatic sulfide-rich nickel-copper-(platinum-group element) deposits related to mafic and ultramafic dike-sill complexes: Chapter I in Mineral deposit models for resource assessment. USGS.

SRK Consulting (2011) Technical Report Nkamouna and Mada deposits https://www.sec.gov/Archives/edgar/data/1398005/000119312511161283/dex991.htm.

Taylor CD, et al. (2013) Descriptive models, grade-tonnage relations, and databases for the assessment of sediment-hosted copper deposits—With emphasis on deposits in the Central African Copperbelt, Democratic Republic of the Congo and Zambia. USGS Scientific Investigations Report, pp 154.

United States Geological Service, Mineral Commodity Summary, U.S. Geological Survey, Reston, Virginia: 2019.

Wells MA, et al. (2009) Mineralogy and crystal chemistry of “garnierites” in the Goro lateritic nickel deposit, New Caledonia, Eur J Mineral 21:467–483

Germanium and cobalt in sedimentary rock-hosted deposits of northwestern Alaska

Garth E. Graham, Karen D. Kelley
U.S. Geological Survey, USA

Abstract. Cobalt and germanium are critical elements that are essential for a number of technological applications. Northern Alaska hosts several deposits and occurrences that contain significant amounts of these elements. For example, whole rock geochemistry data show that the clastic-dominated Pb-Zn Anarraaq deposit contains up to 820 ppm Ge (median 110 ppm) and samples from the Bornite carbonate-hosted Cu (Pb-Zn) deposit contain tens of thousands of ppm Co. Mineral chemical data indicate that the Ge is hosted primarily in sphalerite in the Pb-Zn systems but the Ge concentrations vary greatly, due in part to a zoning in sphalerite and/or a complex paragenesis with multiple stages of sphalerite with variable Ge contents. Establishing the paragenesis and mineral chemistry in both Pb-Zn and Cu deposits is important for understanding the deportment of the critical elements like Ge (and Co). The deposits in northern Alaska are significant potential sources of Co and/or Ge, should they ultimately be developed.

1 Introduction

Globally, sedimentary rock-hosted lead-zinc and carbonate-hosted polymetallic deposits are potential sources for a number of critical elements including Co, Ga, Ge, and In (e.g., Marsh et al., 2016; Schulz et al., 2017), which are becoming increasingly important. Cobalt is mostly used in cathodes in rechargeable batteries and in superalloys for jet engines. Germanium is an important component in fiber optic cable and solar arrays, among other applications. In sedimentary rock-hosted deposits, cobalt typically resides as cobaltiferous pyrite and/or other cobalt-bearing minerals. Germanium can occur in Ge-bearing minerals (e.g., renierite, germanite) or as lattice substitutions or nano inclusions in sulfide minerals, particularly sphalerite.

The United States has limited domestic production of both Co and Ge, and thus is highly reliant on international sources (USGS, 2019). Identification of additional domestic sources for these metals is in the national interest. Northern Alaska contains two types of sedimentary rock-hosted deposits that are known to contain significant Co and/or Ge. The clastic-dominated Pb-Zn (CD Pb-Zn) systems include the world-class Red Dog deposit and satellite deposits (Anarraaq, Lik), and the Drenchwater deposit to the east. The carbonate-hosted polymetallic deposits include the Cu-rich Bornite (Ruby Creek) and Omar prospect, along with a number of additional Pb-Zn dominated occurrences in the Baird Mountains. In this contribution, we summarize reconnaissance USGS geochemical results that demonstrate known and potential deposits/occurrences that contain enrichments of Co or Ge that could be resources under appropriate market conditions.

2 Geologic background

The CD Pb-Zn deposits (commonly termed SEDEX) of northern Alaska are hosted in Paleozoic passive margin black shales/mudstones with locally abundant carbonate turbidites and chert of the Mississippian Kuna Formation (Fig. 1).

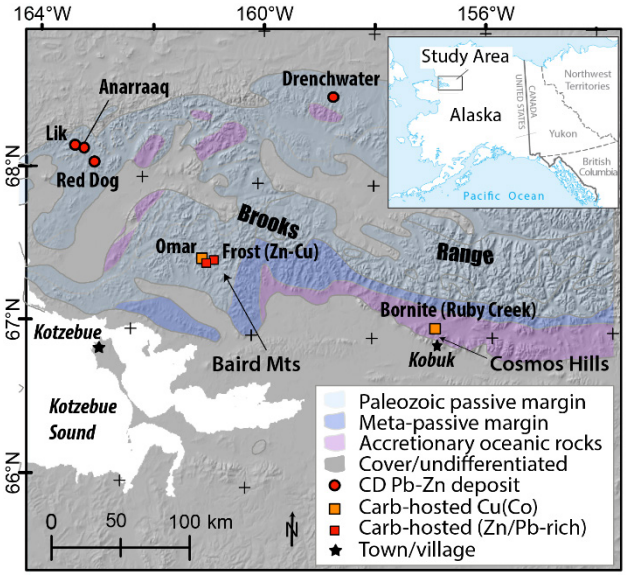

Figure 1. Generalized geology and select Zb-Pb and carbonate-hosted base metal deposits map of northwestern Alaska.

These deposits occur in one of several tectono-stratigraphic assemblages of dominantly sedimentary rocks that were juxtaposed during the Late Jurassic to Tertiary Brookian orogeny on the northern edge of the Brooks Range. (e.g., Moore et al., 1994). Voluminous volcanic and intrusive plugs are recognized only in the vicinity of the Drenchwater deposit, located ~200 km east of Red Dog (Werdon, 1996). Mineralised rocks in ore zones contain laminated to chaotic semi-massive to massive sulfides typically dominated by sphalerite, with lesser galena and pyrite. At some deposits (e.g., Red Dog), vein ores are economically significant. Multiple sphalerite stages are recognized at Red Dog and Anarraaq (Kelley et al., 2004a,b, Smith, 2017). Both deposits are interpreted to have formed in the shallow subsurface through precipitation of sulfides from basinal brines by replacement of barite and/or carbonate in the clastic-dominated stratigraphy.

Table 1. Summary statistics for whole rock samples from select CD Pb-Zn and carbonate-hosted polymetallic deposits of northwestern Alaska. Data (except Ga) for Red Dog, Anarraaq, and Drenchwater (DW) are from Graham et al. (2009). These data are part of an Alaska statewide compilation (Granitto et al., 2013). Average crustal abundance values from Wedepohl (1995). All values are in parts per million (ppm).

	Co			Cu			Ga			Ge			Pb			Zn		
Deposit(# samps)	Min	Median	Max	Min	Median	Max	Min	Mediar	Max	Min	Median	Max	Min	Median	Max	Min	Median	Max
CD Pb-Zn																		
Red Dog (19)	<1	29	97	<10	140	480	0.5	3	25	1.3	16	60	640	25200	163000	29000	133000	371000
Anarraaq (11)	<1	7	145	<10	12	163	0.5	1	18	16	110	820	980	66900	124900	84400	199000	464500
DW (12)	7	15	44	69	130	740	1	13	49	8	23	88	236	5910	178000	1730	140000	249000
Carb.-hosted																		
Bornite (21)	9	176	16300	129	43500	571000	<1	1	24	<0.5	2.2	48	23.5	150	410	16	166	217000
Baird Cu (14)	<1	132	4320	3630	44600	343000	<0.02	0.3	9.7	<0.5	8.3	110	<5	180	2500	70	1500	16600
Baird-Zn (22)	<1	1	935	6	83	1090	<0.02	4.9	22.7	<0.5	11	98	22.6	1760	70100	12800	82700	484000
Baird Zn-Cu (4)	<1	1	3	1990	7780	40500	43	64	111	9.1	22	91	11	27	130	105000	253000	306000
Baird-Pb (4)	<1	1	2	21	33.55	288	1.6	2.2	9	1.9	2	2.3	12700	49650	59400	2640	2985	6370
Crustal avg.		24			25			15			1.4			14.8			65	

The Cu to Zn-rich carbonate-hosted polymetallic systems are located on the southern side of the Brooks Range (Fig. 1). The largest of these is the Bornite (Ruby Creek) deposit, located in the Cosmos Hills, and hosted in a 1-km-thick sequence of Silurian and Devonian metacarbonates (Hitzman et al., 1986). Mineralisation occurred in synsedimentary or later breccias and involved replacement of breccia matrix and early pyrite by copper minerals, minor sphalerite and galena and carrolite, and lesser reneirite and germanite (Bernstein and Cox, 1986, Hitzman et al. 1986). Mineralisation is interpreted to predate regional greenschist metamorphism. The Omar deposit, a copper-rich orebody located 180 km west of Bornite in the Baird Mountains, is a possible analog, with high cobalt concentrations (Fig. 1; Jansons, 1982; Folger and Schmidt, 1986). Several Zn(Pb) dominated prospects occur in the vicinity of Omar, sometimes with significant Cu (Frost occurrence labeled as Baird Zn-Cu in Fig. 1).

3 Reconnaissance whole rock geochemistry

Whole rock geochemical data for select deposits and occurrences are summarized in Table 1. These data indicate highly variable enrichments of Co and/or Ge. Cobalt concentrations are generally not enriched in CD Pb-Zn deposits (max 145 ppm, median concentrations <30 ppm; Table 1) compared to average continental crust. However, cobalt is highly enriched in some samples from both the Bornite deposit and the Omar Cu prospect, in the Baird Mountains (maximum 16,300 and 4,320 and median concentrations of 176 and 132 ppm, respectively).

Gallium concentrations approximate or are lower than crustal averages in CD Pb-Zn samples (median concentrations of 1 to 16.5 ppm), but a maximum concentration of 49 ppm was reported in mineralised tuff at Drenchwater (Table 1). Ranges are similar in most of the carbonate-hosted systems, although four Zn and Cu-rich surface samples at the Frost occurrence near Omar yielded 43 to 111 ppm Ga. Based on our limited dataset from the Bornite deposit, the highest Ga concentrations of 15 to 24 ppm occurred in poorly mineralised shale.

The Anarraaq deposit has distinctly elevated Ge concentrations, with maximum and median concentrations of 820 and 110 ppm, respectively from grab samples, consistent with previous reports (Jennings and King, 2002). Red Dog and Drenchwater CD Pb-Zn deposits have significantly lower median concentrations of ~16 and 23 ppm, respectively. Germanium concentrations are also elevated at Frost (Baird-Zn-Cu on Table 1).

4 Mineral chemistry

Mineral chemistry data are available for a few of the CD Pb-Zn deposits but not the carbonate-hosted deposits considered here. At the Red Dog deposit, four different paragenetic stages of sphalerite are recognized, including stage 2 yellow-brown sphalerite and stage 3 red-brown sphalerite that together comprise the majority of the ore (Kelley et al., 2004a). Median concentrations of 149, 103, 82, 247 ppm Ge in these stages, were established by laser ablation inductively coupled mass spectrometry (LA-ICP-MS). Stage 2 and 3 sphalerite also contains median concentrations of Co of 102 and 149 ppm, higher than pyrite associated with these generations (median 60 and 7 ppm, respectively).

Germanium concentrations in sphalerite samples from other deposits, including Anarraaq, Drenchwater and Lik are summarized in Graham et al. (2009). Limited sphalerite chemical data for Anarraaq indicate high Ge concentrations (median ~420 ppm) relative to 94 to 140 ppm median value for other deposits, including volumetrically dominant stages 2 and 3 at Red Dog (Fig. 2). More recently, Smith (2017) established qualitatively significant variations in Ge concentrations in different generations of sphalerite from Anarraaq.

Elemental associations of Ge differ among stages and deposits. For example, despite some data scatter, Ag displays a positive correlation with increasing Ge associated with different stages of sphalerite at Red Dog. In contrast, Anarraaq samples show no systematic relationship between Ge and Ag, but Ge displays positive correlation with Mn and Tl concentrations (the absolute concentrations of which are higher than those at Red

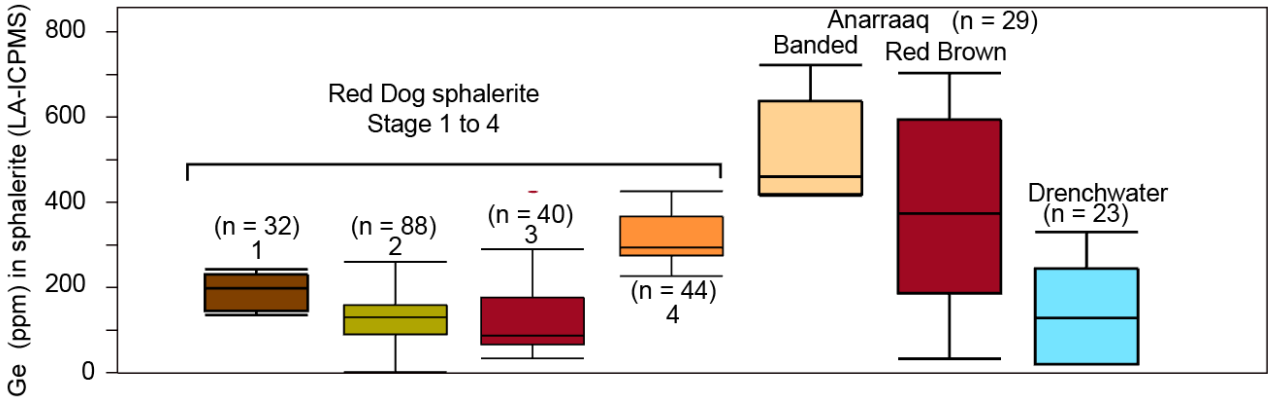

Figure. 2. Boxplots showing the ranges of germanium concentrations in LA-ICPMS analyses of sphalerite from the Red Dog, Anarraaq, and Drenchwater CD Pb-Zn deposits. Note the difference in concentration ranges for the better characterized Red Dog sphalerite generations (relatively narrow) versus lesser characterized samples from Anarraaq and Drenchwater. Data included from Graham et al. (2009).

Dog) in two distinctly different sphalerites (banded and red-brown; Fig. 2) from different parts of the deposit.

5 Discussion

5.1 Comparison to domestic production and deposits

The critical mineral endowment of some of the northern Alaskan deposits is significant and could be important for future supply. In 2018, only 500 tonnes of Co were produced in the US (USGS, 2019, page 50). The recent inferred resource estimate of 77 million pounds of Co at Bornite in combined open-pit and underground zones with different Cu cut-off grades (Trilogy Metals, Inc. 2018) equates to approximately 34,900 tonnes of Co. This makes Bornite one of two recently delineated Co-bearing sedimentary-rock hosted deposits in the US (the other being the Black Butte deposit in Montana). The similarity of Omar to Bornite with respect to geology and geochemical signatures opens the potential for additional resources. However, additional extensive work is necessary to assess the potential of this very remote deposit.

Domestic production numbers for Ge are not currently available, although zinc concentrates from the US are sent to Canada for smelting for Ge recovery (USGS, 2019). Some of these ores are assumed to be from Red Dog, which had previously reported concentrations of 79 ppm Ge in zinc concentrate (Alaska Department of Environmental Conservation, Tennessee. Massive sphalerite/sphalerite concentrate chemistry show Ge concentrations appreciably higher than Red Dog, at ~200 to 390 ppm (Bonnett et al., 2016). However, these concentrations are approximately the same as the median values in Anarraaq sphalerite (a proxy for concentrate results).

5.2 Mineral residence

The LA-ICP-MS data for sphalerites demonstrate complex trace element associations both within the paragenetic evolution of a given deposit and among deposits. Even within the well-studied Red Dog deposit significant ranges of Ge exist in each of the four stages. In the more poorly characterized samples used for the reconnaissance work at Anarraaq and Drenchwater, broad ranges in Ge concentrations undoubtedly reflect either zoning within single crystals or treatment of different paragenetic stages as a single population (Fig. 2). The work of Smith (2017) demonstrates major variation in Ge and other trace element concentrations in the different stages, with irregular and patchy character specifically for Ge at the micron to millimeter scale within a single crystal.

These data also suggest that there may be different chemical processes at the stage or deposit scale that control trace element compositions of sphalerite. For example, the positive correlations between Ge and Mn for most Anarraaq sphalerite analyses could be recording a redox control on sphalerite formation. Anaaraaq ores contain abundant organic matter that could have served as a reductant (Kelley et al. 2004b).

The absence of any noted Ge-bearing phases at Anarraaq, despite the high concentrations of Ge contrasts with reports of Ge-bearing (and Co-bearing) phases at Bornite, which contains lower absolute Ge concentrations as suggested by our limited sample suite. Cugerone et al. (2018) suggested that the abundance of accessory Ge-minerals and Ge-poor sphalerite in Variscan Pb-Zn vein deposits was a consequence of recrystallization of sphalerite by a metamorphic overprint that expelled many of the trace element impurities, including Ge. Similar processes may have, at least in part, caused formation of Ge-(and Co-bearing) phases in Bornite. Such greenschist metamorphic conditions have not impacted the CD Pb-Zn deposits. Textural and mineral chemistry analyses from the carbonate-hosted deposits may help answer this question.

6 Conclusions

Geologic evidence demonstrates that there is significant resource potential for both Co and Ge in different sedimentary rock-hosted deposits of northwestern Alaska. Mineral chemistry studies highlight the

complexity of the controls on Ge concentrations on the micro- through macro scales. As society seeks additional critical element resources, it is essential to develop a strong understanding of paragenetic relationships within deposits to define the deportment of elements of interest. Combined with an evolving understanding of why they occur in certain stages we will enhance our capability of predicting where these resources might occur.

Acknowledgements

We thank Jane Hammarstrom and Erin Marsh for their comments on earlier iterations of this abstract.

References

Alaska Department of Environmental Conservation (2002) Table 2-1: Composition of Red Dog lead and zinc concentrates (revised 6-7-05). https://dec.alaska.gov/spar/csp/docs/reddog/03dmts_ra_tables-april2005.pdf. Accessed 22 February 2019

Bernstein LR, Cox DP (1986) Geology and sulfide mineralogy of the Number One Orebody, Ruby Creek copper deposit, Alaska. Econ Geol 81: 1675-1689

Bonnett J, Mosser-Ruck R, Caumon MC, Andre-Mayers AS, Cauzid J, Peiffert C (2016) Trace element distribution (Cu, Ga, Ge, Cd and Fe) in sphalerite from the Tennesssee MVT deposits, USA, by combined EMPA, LA-ICP-MS, Raman spectroscopy, and crystallography. Can Mineral 54:1261-1284

Cugerone A, Cenki-Tok B, Chauvet A, Le Goff E, Bailly L, Alard O, Allard M, (2018) Relationships between occurrence of accessory Ge-minerals and sphalerite in Variscan Pb-Zn deposits of the Bossost anticlinorium, French Pyrenean Axial Zone: chemistry, microstructures and ore-deposit setting. Ore Geol Rev 95:1-19

Folger PF, Schmidt JM (1986) Geology of the carbonate-hosted Omar copper prospect, Baird Mountains, Alaska: Econ Geol 81:1690-1695

Graham GE, Kelley KD, Slack JF, Koenig, A**E** (2009) Trace elements in Zn-Pb-Ag deposits and related stream sediments, Brooks Range Alaska, with implications for Tl as a pathfinder element. Geochem: Explor Environ Anal 9:19-37

Granitto M, Schmidt JM, Shew NB, Gamble BM, Labay KA (2013) Alaska Geochemical Database, Version 2.0 (AGDB2)—including “best value” data compilations for rock, sediment, soil, mineral, and concentrate sample media. US Geol Surv Data Series 759:20 pamphlet and database, 1 DVD, https://pubs.usgs.gov/ds/759/

Hitzman MW, Proffett JM, Schmidt, J, Smith TE (1986) Geology and mineralization of the Ambler District northwwestern Alaska. Econ Geol 81:1592-1618

Jansons U (1982) Cobalt content in samples from the Omar copper prospect, Baird Mountains, Alaska, US Geol Surv Open File Report MLA 109-82:16 http://dggs.alaska.gov/webpubs/usbm/mla/text/mla109_82.pdf. Accessed 25 February 2019

Jennings S, King AR (2002) Geology, exploration history and future discoveries in the Red Dog district, western Brooks Range, Alaska. In Cooke D, Pongratz J (eds) Giant Ore Deposits: Characteristics, genesis and exploration, Center for Ore Deposit Research, Hobart Australia, pp. 151–158

Kelley KD, Leach DL, Johnson CA, Clark JL, Fayek M, Slack JF, Anderson VM, Ayuso RA, Ridley WI (2004a). Textural, Compositional, and Sulfur Isotope Variations of Sulfide Minerals in the Red Dog Zn-Pb-Ag Deposits, Brooks Range, Alaska: Implications for Ore Formation. Econ Geol *99*:1509–1532

Kelley KD, Dumoulin JA, Jennings S (2004b). The Anarraaq Zn-Pb-Ag and barite deposit, northern Alaska: Evidence for replacement of carbonate by barite and sulfides. Econ Geol *99*:1577–1591

Marsh EE, Hitzman MW, Leach DL (2016) Critical elements in sediment-hosted (clastic-dominated Zn-Pb-Ag, Mississippi Valley Type Zn-Pb, sedimentary rock-hosted stratiform Cu, and carbonate-hosted polymetallic deposits): A review. Rev Econ Geol 18: 307-321

Moore TE, Wallace WK, Bird KJ, Karl SM, Mull CG, Dillon JT (1994) Geology of northern Alaska. In Plafker , Berg HC (eds) The Geology of Alaska: Geol Society of America, pp. 49-138

Schulz KJ, DeYoung JH Jr, Seal II RR, Bradley DC (eds.) (2017) Critical mineral resources of the United States—Economic and environmental geology and prospects for future supply. US Geol Surv Prof. Paper 1802:797. doi.org/10.3133/pp1802.

Smith D (2017) Lithophile and Chalcophile Elements in Sphalerite from the Anarraaq Sediment-Hosted Zn-Pb-Ag Deposit, Red Dog District, Alaska, Masters thesis, University of Alberta, 117 p

Trilogy Metals Inc., 2018. Trilogy Metals Inc. NI 43-101 Technical Report on the Bornite Project, Northwest Alaska, USA. July 20th 2018 release. https://trilogymetals.com/assets/docs/Technical_Report_for_the_Bornite_Co_Update_2018_07_20-F.pdf. Accessed 22 February 2019

U.S. Geological Survey, 2019, Mineral commodity summaries 2019: US Geol Surv, 200 p., https:// doi.org/10.3133/70202434. ISBN 978-1-4113-4283-5.

Wedepohl KH (1995) The composition of the continental crust. Geochim. Cosmochim. Acta 59: 1217–1232

Werdon MB (1996) Drenchwater, Alaska; Zn-Pb-Ag mineralization in a mixed black shale; volcanic environment, in Coyner, A.R., and Fahey, P.L., eds., Geology and ore deposits of the American Cordillera: Reno, Nev., Geol Soc Nevada Symp Proceed, pp 1341–1354

The genesis of Carlow Castle: a unique Australian orogenic Cu-Co-Au deposit in the Archean Pilbara Craton

David Fox, Samuel Spinks, Mark Pearce, Margaux Le Vaillant, Robert Thorne
CSIRO Mineral Resources, Australian Resources Research Centre, Australia
David Fox, Milo Barham, Mehrooz Aspandiar
The Institute for Geoscience Research (TIGeR), School of Earth and Planetary Sciences, Curtin University, Australia

Abstract. Carlow Castle is a Cu-Co-Au deposit situated within the western Pilbara Craton of Western Australia. Whilst Carlow Castle is the oldest discovered copper deposit in the Pilbara region, having been initially discovered in 1882 (Ruddock 1999), no detailed study of the ore mineralisation has ever been undertaken. After being long abandoned, a recent drilling campaign through 2018 uncovered an economically significant and geologically complex system of Cu-Co-Au mineralisation with a current resource estimate for Carlow Castle of 7.7Mt @ 1.06g/t Au, 0.51% Cu, and 0.08% Co (Artemis Resources Limited 2019), making it one of Australia's most significant Cu-Co-Au deposits. Recent analysis suggests that Carlow Castle is a hydrothermal Cu-Co-Au deposit, with mineralisation hosted in sulphide-rich quartz veins throughout a pervasively chloritised shear zone in an Archean mafic volcano-sedimentary sequence. Within these ore veins, the sulphide mineralogy is dominated by pyrite (FeS_2), chalcopyrite ($CuFeS_2$), chalcocite (Cu_2S), and cobaltite (CoAsS). Here we present the findings of the first detailed study on the nature of the Cu-Co-Au mineralisation at Carlow Castle and propose an orogenic model for the genesis of this unique deposit.

1 Introduction

The Carlow Castle Cu-Co-Au deposit occurs in the West Pilbara region of Western Australia, ~10 km SW of Roebourne, ~25 km SE of Karratha, and ~1500 km NE of Perth. The present JORC (2012) compliant resource for Carlow Castle is 7.7 Mt @ 1.06 g/t Au, 0.08% Co, and 0.51% Cu (Artemis Resources Limited 2019); making this one of Australia's most significant Cu-Co-Au deposits (Britt et al. 2017). This follows major exploration and drilling campaigns by Artemis Resources through 2017 and 2018 resulting in the discovery of this resource proximal to the previously abandoned Carlow Castle Cu mine. Here it is proposed that Carlow Castle's genesis most closely matches the conventional genetic model for an orogenic Au deposit, however its particularly cobaltiferous ore mineralisation makes it unique among orogenic Au deposits, which are not commonly observed to be strongly enriched in Co (Groves et al. 1998). This is topical given the present broad interest in Co as a critical battery metal and the increasing drive for Co exploration to ensure security of supply as the adoption of electric vehicles increases and renewable energy storage becomes of greater importance to the global energy industry (Olivetti et al. 2017). The necessity to better understand the genesis of Co mineralisation is additionally compounded by existing risks in the supply security of Co pertaining to the fact that >50% of Co is presently sourced from the Democratic Republic of Congo (US Geological Survey 2018). Given the economic significance of this deposit, the current broad interest in Co deposits, the recency of this discovery, its unique Cu-Co enrichment, and the lack of any existing literature on this deposit this study introduces this unique class of Co-rich orogenic Au deposits with insights into the genesis of Carlow Castle specifically. It is anticipated that by providing insights into the unique combination of processes required to form Co-rich orogenic Au deposits, and determining how these differ from conventional orogenic Au genetic models, that exploration for these deposits can be enhanced.

2 Geological background

The Pilbara Craton is an Archean craton that covers ~400,000 km^2 in the northwest region of Western Australia and is divided broadly into the Archean North Pilbara granite-greenstone terrain (3.6-2.8 Ga) and the overlying Mount Bruce Supergroup of Archean to Paleoproterozoic age (2.77-2.3 Ga), which primarily occurs along the southern edge of the craton within the Hammersley and Fortescue Basins (Ruddock 1999; Smithies et al. 1999; Van Kranendonk et al. 2002). Carlow Castle is hosted in a volcano-sedimentary sequence within the West Pilbara Superterrane of the northwest Pilbara Craton (Hickman 2016). This volcano-sedimentary sequence is denoted as the Ruth Well Formation; forming part of the Roebourne Group, which is in turn a component of the Karratha Terrane (Hickman 2016; Ruddock 1999). Within the Ruth Well Formation, the mineralisation at Carlow Castle occurs proximal to the Regal Thrust; a regionally significant thrust fault that is interpreted to have formed immediately before or during the original formation of the West Pilbara Superterrane (3.16-3.07 Ga) (Hickman 2016; Van Kranendonk et al. 2007). This may have coincided with the Prinsep Orogeny, where obduction of the Regal Formation onto the Karratha Terrane formed the Regal Terrane and the continued convergence of the Regal Karratha, Regal, and Sholl terranes caused their amalgamation into the West Pilbara Superterrane (Hickman 2016). This was followed by the collision of the West Pilbara Superterrane and the East Pilbara Terrane from ~3.068-3.066 Ga (Hickman 2016).

3 Cu-Co-Au mineralisation

3.1 Style of mineralisation

The mineralisation at Carlow Castle deposit is hosted in a heavily altered dominantly mafic volcano-sedimentary sequence, within the Ruth Well Formation (Ruddock 1999). With this considered, it is often difficult to constrain the primary lithology within which Carlow Castle's mineralisation is hosted due to extensive hydrothermal alteration that has produced a pervasively chloritised and silicified host lithology. However, based on previous studies of the Ruth Well Formation, it is likely that this host lithology was dominated by a volcanic sequence of mafic to ultramafic rocks with minor chert and carbonaceous shale beds (Hickman 2016; Ruddock 1999; Van Kranendonk et al. 2006). Within the Ruth Well Formation, the Co-Cu-Au mineralisation typically occurs within 100 m of the surface and this mineralisation occurs broadly in two styles. The first, and most significant, style of mineralisation is structurally-hosted, where mineralisation occurs in quartz-carbonate and sulphide veins through brecciated and sheared basalt. The second style of mineralisation occurs near to the surface, overlying the structurally-hosted sulphide mineralisation, as an oxidised supergene layer. Within this oxidised layer, there is partial to complete replacement of the original sulphide mineralisation with secondary Cu-oxide and carbonate minerals.

3.2 Structure and extent

Carlow Castle occurs within a heavily tectonised zone through the Ruth Well Formation, proximal to the regionally significant Regal Thrust. Reflecting this, the Ruth Well Formation at Carlow Castle hosts evidence of several generations of deformation. Brittle deformation is intense through portions of Carlow Castle, where the Ruth Well Formation proximal to the ore zone is heavily brecciated and this brecciation forms a network of quartz infilled fractures. In addition to these brittle structures, there is also extensive evidence of ductile deformation at Carlow Castle, where quartz and sulphide veins throughout the Ruth Well Formation in portions of the ore zone are heavily sheared and folded. These brittle and ductile structures at Carlow Castle are both observed to host mineralisation, which occurs infilling these structures as networks of quartz-sulphide veins. The formation of these structures was clearly critical to the genesis of this mineralisation as they provided permeable structures to allow Carlow Castle to act as a regional focus for migrating mineralising fluids. This includes those that may have flowed along the proximal Regal Thrust, to which gold mineralisation is more broadly associated (Hickman 2016).

3.3 Mineralogy

The structurally-hosted mineralisation at Carlow Castle occurs broadly in two sulphide-dominated mineral assemblages. The first of these is a chalcocite-cobaltite-gold assemblage, whilst the second is composed predominantly of a pyrite-chalcopyrite assemblage. In addition to these minerals, other minerals are observed to occur in these assemblages in minor or trace volumes. These mineral assemblages are summarised in Table 1.

Table 1. Summary of two distinct ore mineral assemblages that occur through Carlow Castle Cu-Co-Au deposit.

	Mineral Assemblage One	Mineral Assemblage Two
Cu	Chalcocite (Cu_2S), ±Chalcopyrite ($CuFeS_2$)	Chalcopyrite, ±Chalcocite
Co	Cobaltite (CoAsS)	± Cobaltite
Au	Gold (Au)	± Gold
Other	±Pyrite (FeS_2), ±Uraninite (UO_2)	Pyrite, ±Tellurobismuthite (Bi_2Te_3), ±Hessite (Ag_2Te)

The two mineral assemblages appear to occur independently of one another; they do not appear to reflect a broad scale mineralogical or geochemical zonation within the ore body at Carlow Castle. With this considered, Assemblage Two forms the majority of the structurally-hosted sulphide mineralisation throughout Carlow Castle, whilst Assemblage One occurs primarily in vein networks that are limited to the particularly Cu, Co, Au-rich portions of Carlow Castle.

Petrographic analysis of the sulphide mineralisation within the Carlow Castle ore body provide insights into the genesis of this mineralisation. Within Assemblage One (Fig. 1) the dominant sulphide minerals are chalcocite and cobaltite, occurring in varying amounts from almost entirely cobaltite to almost entirely chalcocite. Generally, within these veins cobaltite occurs as aggregates of euhedral-subhredral crystals hosted in a mix of quartz and siderite. Networks of thin chalcocite veinlets commonly occur through these cobaltite-rich veins, typically surrounding cobaltite grains and filling in networks within these larger quartz-carbonate veins.

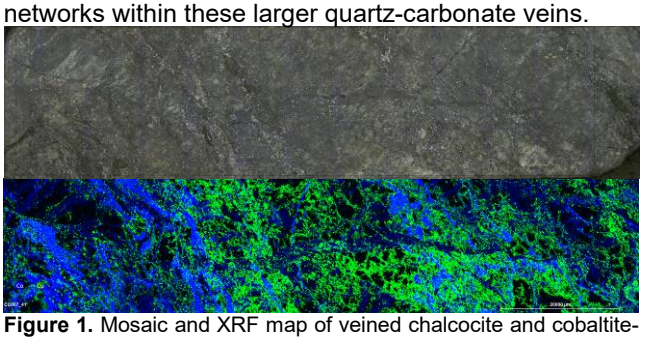

Figure 1. Mosaic and XRF map of veined chalcocite and cobaltite-rich Assemblage One. Note here that on the XRF map green corresponds to Cu and blue corresponds to Co. This sample is ~22 cm long.

Notably, there is a clear genetic relationship, within this assemblage, between cobaltite and gold mineralisation as the native gold is observed to occur virtually exclusively as inclusions within grains of cobaltite. Additionally, trace inclusions of chalcopyrite and uraninite are also observed within these grains of cobaltite. Finally, it is interesting to note that pyrite, when it does occur within this assemblage, is commonly observed to be partially replaced by chalcocite; where chalcocite surrounds pyrite and occurs as penetrating lamellae throughout.

Assemblage Two (Fig 2.) is defined by an intergrown assemblage that is primarily composed of chalcopyrite

and pyrite. Where this assemblage occurs in in quartz-carbonate veins, pyrite and chalcopyrite tend to be anhedral and form stringy veinlet networks infilling space between quartz. These veinlet network of chalcopyrite and pyrite are occasionally associated with blocky grains of euhedral to subhedral cobaltite. Assemblage Two also occurs in particularly sulphide-rich veins where gangue quartz-carbonate is limited and instead the chalcopyrite and pyrite compose virtually all of these veins, here these sulphides are massive with intergrown anhedral pyrite and chalcopyrite but are commonly also intergrown with chlorite from the pervasively altered host rock. Interestingly, in massively textured samples of Assemblage Two, cobaltite is less common in comparison to the more quartz-rich veinlet textured samples. Further within assemblage Two, gold is notably less common in general in comparison to Assemblage One. However, gold does occur within Assemblage One in trace quantities and it is commonly associated with chalcopyrite. Finally, there is a clear association between the tellurides hessite and tellurobismuthite and pyrite as these tellurides occur exclusively as inclusions within pyrite.

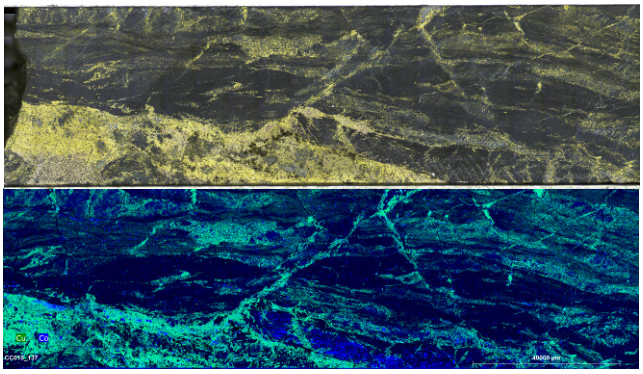

Figure 2. Mosaic and XRF map of veined chalcopyrite and pyrite-rich Assemblage Two with minor cobaltite. Note that on the XRF map green corresponds to Cu and blue corresponds to Co. This sample is ~20 cm long.

3.4 Geochemistry

Strong enrichments are observed in Cu, Co, Au at Carlow Castle. Several interesting relationship are observed between elements within the ore body; most notably correlation coefficients of 1.00 for Co:As, 0.95 for Ag:Cu, 0.83 for Au:Co, 0.69 for Au:Cu, 0.61 for Cu:Co. The perfect positive correlation between Co and As confirms mineralogical observations that all of the Co within the deposit is hosted in cobaltite. Additionally, the strong positive correlation between Au and Co provides additional geochemical evidence of the previously mentioned genetic relationship between Co and Au mineralisation observed in Assemblage One. Conversely, the comparably less strong positive correlation between Co and Cu suggests that these two metals do not always occur in association, as has been observed mineralogically above.

4 Genesis

As no detailed study of Carlow Castle has previously been conducted, very little beyond superficial ideas regarding the metallogeny of this deposit exist (Hickman 2016; Ruddock 1999). With this considered, the interpretation proposed here is that Carlow Castle represents an orogenic hydrothermal Cu-Co-Au deposit, this is congruent with suggestions regarding Carlow Castle's genesis posited by Ruddock (1999) and Hickman (2016) based on broad-scale observations. This is proposed due to the fact that Carlow Castle exhibits several geological characteristics that are typical of orogenic gold deposits. On a broad scale, the first of these characteristics is Carlow Castle's regional situation in an Archean greenstone belt and, on a smaller scale, within a rift-related volcano-sedimentary succession (Groves et al. 1998; Hickman 2016; Van Kranendonk et al. 2010). Additionally, the occurrence of Carlow Castle within the West Pilbara Superterrane, a collisional accretionary superterrane that formed at ~3.068 Ga during the Prinsep Orogeny (Hickman 2016), provides a classic tectonic setting for an orogenic gold system (Goldfarb et al. 2001; Groves et al. 1998). On a deposit scale, the strong structural control on mineralisation, occurrence through a heavily tectonised zone proximal to the regionally significant Regal Thrust fault, pervasive quartz-carbonate veining, extensive chloritic hydrothermal alteration, and the otherwise clear hydrothermal origin of Carlow Castle are similarly typical of orogenic mineral systems (Saunders et al. 2014; Groves et al. 1998; Goldfarb et al. 2001).

As Carlow Castle has been classified here as an orogenic Cu-Co-Au deposit, its genesis is inextricably linked to the ~3.068 Ga Prinsep Orogeny during the amalgamation of the Karratha, Regal, and Sholl Terranes into the West Pilbara Superterrane and the subsequent convergence of the West Pilbara Superterrane and the East Pilbara Terrane (Van Kranendonk et al. 2007; Hickman 2016). Given its close proximity to the Regal Thrust, which is believed to have formed during the Prinsep Orogeny or the prior convergent 'Karratha Event' around ~3.16 Ga (Hickman 2004; Van Kranendonk et al. 2010), the formation of this thrust and the associated tectonization at Carlow Castle was key to the genesis of the Cu-Co-Au mineralisation. This is because although the timing of the mineralisation at Carlow Castle is not yet constrained relative to these tectonic events and the formation of the Regal Thrust, the Regal Thrust and the tectonised zone at Carlow Castle were at very least key to the genesis of this mineralisation in that they provided conduits and a regional fluid focus for migrating ore fluids. Whilst the source of these fluids and their metal enrichment is not yet constrained, Hickman (2016) suggested that the proximal sediments of the Nickol River Formation may have provided a source of gold due to the deposition of detrital gold into these sediments; shed from eroded gold deposits in the East Pilbara Terrane. However, there is no strong evidence to directly support this hypothesis and further study is required to constrain the metal source for Carlow Castle. With this considered, the uniquely strong enrichment of Co and Cu in this deposit implies a unique metal source relative to other orogenic Au systems. If the formation of this mineralisation was synchronous to the Prinsep Orogeny

then it is likely that this ore fluid would have been produced by metamorphic devolatilization (Cox 2005; Tomkins 2013). The Cu-Co-Au rich ore fluid would have been channeled through permeable structures along the Regal Thrust and focused into the brecciated and sheared zone at Carlow Castle. Once channeled into third-order structures, metal deposition would have most likely occurred due to wall rock interaction with the mafic volcanic rocks and carbonaceous shales of the Ruth Well Formation (Morey et al. 2007; Phillips and Powell 2010; Hickman 2016).

5 Implications

The primary significance of Carlow Castle stems from its unique Cu-Co-Au metal association and its unique ore mineralogy given its interpreted genesis as an orogenic Au deposit. Although Carlow Castle does bear some broad mineralogical, textural, or structural similarities to other rare examples of Co mineralisation in some orogenic terranes (e.g. Bou Azzer, Morocco and Idaho Cobalt Belt, USA), Carlow Castle is distinguished by its Archean age; significant Cu-Au enrichment; and lack of Ni enrichment. Given the recency of the discovery of major structurally-hosted Cu-Co-Au mineralisation at Carlow Castle (Artemis Resources Limited 2019), the purpose of this research is to provide the first overview of the geology of Carlow Castle and nature of its mineralisation, as there is no other existing literature focused on Carlow Castle. This work is particularly topical due to the strong Co enrichment within Carlow Castle and the current broad interest in Co deposits due to the dramatic increase in Co prices through 2017 and 2018 (London Metal Exchange 2019), driven by projections of increased demand from the battery sector due to Co's status as a key metal in Li-ion batteries (US Geological Survey 2018). Because of its unique enrichment in Cu and Co, understanding the unique combination of processes necessary to form this deposit and how they differ from the conventional model for orogenic Au deposits are of broad significance as they could assist with exploration efforts for other cobaltiferous orogenic Au deposits. This is particularly significant given the present lack of supply security for cobalt.

Acknowledgements

This research was supported by an Australian Government Research Training Program Scholarship and a CSIRO Mineral Resources postgraduate student scholarship. Artemis Resources Ltd. are acknowledged for their financial, logistical, and material support.

References

Artemis Resources Limited (2019) Carlow Castle Au-Cu-Co Resource Grows by 71% to 7.7Mt.

Britt A, et al. (2017) Australia's Identified Mineral Resources 2017. Geoscience Australia, Canberra.

Cox SF (2005) Coupling between Deformation, Fluid Pressures, and Fluid Flow in Ore-Producing Hydrothermal Systems at Depth in the Crust. Economic Geology 100th Anniversary Volume:39-75.

Goldfarb RJ, et al. (2001) Orogenic gold and geologic time: a global synthesis. Ore Geology Reviews 18:1-75.

Groves DI, et al. (1998) Orogenic gold deposits: A proposed classification in the context of their crustal distribution and relationship to other gold deposit types. Ore Geology Reviews 13:7-27.

Hickman AH (2004) Two contrasting granite−greenstone terranes in the Pilbara Craton, Australia: evidence for vertical and horizontal tectonic regimes prior to 2900 Ma. Precambrian Research 131:153-172.

Hickman AH (2016) Northwest Pilbara Craton: a record of 450 million years in the growth of Archean continential crust. Geological Survey of Western Australia, Perth, pp 104.

JORC (2012) Australasian Code for Reporting of Exploration Results, Mineral Resources and Ore Reserves. The Joint Ore Reserves Committee of The Australasian Institute of Mining and Metallurgy, Australian Institute of Geoscientists and Minerals Council of Australia.

London Metal Exchange (2019) LME Cobalt. London Metal Exchange.

Morey A, et al. (2007) The structural controls of gold mineralisation within the Bardoc Tectonic Zone, Eastern Goldfields Province, Western Australia: implications for gold endowment in shear systems. Mineralium Deposita 42:583-600.

Olivetti EA, et al. (2017) Lithium-Ion Battery Supply Chain Considerations: Analysis of Potential Bottlenecks in Critical Metals. Joule 1:229-243.

Phillips GN, Powell R (2010) Formation of gold deposits: a metamorphic devolatilization model. Journal of Metamorphic Geology 28:689-718.

Ruddock I (1999) Mineral occurences and exploration potential of the west Pilbara. Western Australia Geological Survey, Perth, Western Australia, pp 63.

Saunders JA, et al. (2014) 13.15 - Geochemistry of Hydrothermal Gold Deposits In: Holland H, Turekian K (eds) Treatise on Geochemistry. 2 edn. Elsevier, Amsterdam, pp 383-424.

Smithies RH, Hickman AH, Nelson DR (1999) New constraints on the evolution of the Mallina Basin, and their bearing on relationships between contrasting eastern and western granite–greenstone terranes of the Archaean Pilbara Craton,Western Australia. Precambrian Research 94:11-28.

Tomkins AG (2013) On the source of orogenic gold. Geology 41:1255-1256.

US Geological Survey (2018) Mineral commodity summaries 2018. U.S. Geological Survey, pp 200p.

Van Kranendonk MJ, Hickman AH, Smithies RH, Nelson DR, Pike G (2002) Geology and Tectonic Evolution of the Archean North Pilbara Terrain, Pilbara Craton, Western Australia. Economic Geology 97:695-732.

Van Kranendonk MJ, Hickman AH, Smithies RH, Williams IR, Bagas L, Farrell TR (2006) Revised lithostratigraphy of Archean supracrustal and intrusive rocks in the northern Pilbara Craton, Western Australia. Western Australia Geological Survey, pp 57p.

Van Kranendonk MJ, Smithies RH, Hickman AH, Champion D (2007) Review: secular tectonic evolution of Archean continental crust: interplay between horizontal and vertical processes in the formation of the Pilbara Craton, Australia. Terra Nova 19:1-38.

Van Kranendonk MJ, Smithies RH, Hickman AH, Wingate MTD, Bodorkos S (2010) Evidence for Mesoarchean (~3.2Ga) rifting of the Pilbara Craton: The missing link in an early Precambrian Wilson cycle. Precambrian Research 177:145-161.

Potential for low cost bioprocessing of Co and Ni from Nkamouna lateritic ore.

D. Sulaiman J. Mulroy[1,2], Victoria S. Coker[1], Jonathan R. Lloyd[1], Paul F. Schofield[2], J. Fred W. Mosselmans[3]
[1]*The University of Manchester,*
[2]*The Natural History Museum*
[3]*Diamond Light Source*

Abstract. The Nkamouna laterite, S.E. Cameroon, a uniquely Co-Ni enriched laterite hosts ~54Mt of proven and probable ore reserves. Co and Ni, plus local enrichments of Ba (≤1wt%) and Ce (≤0.35wt%), are associated with Mn(III/IV)-oxides e.g. lithiophorite, asbolane, and hollandite group phases. Biostimulation of indigenous microbial communities with a carbon source (glucose) under anaerobic conditions promoted generation of organic acids, e.g. acetate, through fermentation and provided dissimilatory metal reducing bacteria (DMRB) with potential electron donors to support reduction of Mn^{3+}/Mn^{4+} ore minerals to Mn^{2+} causing release of target metals. In addition to standard geochemical analytical techniques a range of spectroscopic techniques have been used to confirm; 1) the mineralogy of the deposit with respect to Co, Ni and Ce and; 2) the divalent oxidation state of solid and soluble Co (and Mn) products generated through bioreduction of the ore. Complementary experiments on synthetic phases, e.g. Co-Ni-asbolane, with pure cultures of the DMRB *Geobacter sulfurreducens* showed total dissolution of the mineral phase. Preliminary results indicate a potential method for bioprocessing of the ore utilising organic carbon as the energy source and on scale-up could supplant glucose with low-cost organics e.g. cellulosic agricultural waste reducing reagent costs for metal extraction.

1 Introduction

Cobalt (Co) has been labelled "critical" by various national/supranational institutions (Slack et al. 2017; European Commission. 2017) and is ranked 10th out of 41 elements in terms of supply risk (BGS. 2015). 2018 supply was dominated the Democratic Republic of Congo (~60%) (Shedd. 2019) however historical political instability has previously caused supply shortages and elevated prices (Slack et al. 2017; Mudd et al. 2013). Concerns regarding the trade of conflict minerals at times mined using child labour (Diemel. 2018; de Haan and Geenen. 2016) have highlighted the importance of finding other sources of Co. Production has increased significantly from 1960 (~14.2kt) to 2018 (~140kt) (Kelly and Matos. 2017; Shedd. 2019) and demand is likely to increase further due to requirements for environmental- and hi-tech applications (Roberts and Gunn. 2013) such as superalloys for gas turbines and jet engines (Mouritz. 2012), rechargeable batteries for electric cars and electronics (Nitta et al. 2015; Perner and Vetter. 2015), catalysts for petrochemical processing (Javadli and de Klerk. 2012) and emerging uses e.g. magnetic nanoparticles (Johannsen et al. 2005; Byrne et al. 2013) all serving an increasing world population with growing energy demands (United Nations. 2015; United Nations. 2018).

A potential alternative source is the Nkamouna laterite in S.E. Cameroon (Lambiv-Dzemua et al. 2013) which is the focus of this work. Bioprocessing methods for other lateritic ores have attracted recent attention as low-cost alternatives to conventional hydrometallurgical processes. Initial studies have focused on bioleaching with sulphuric acid generated from sulphur by acidophilic bacteria, e.g. *Acidithiobacillus* (Smith et al. 2016). Bioleaching via biostimulation of indigenous anaerobic neutraphiles remains a poorly characterized alternative. Here, organic carbon, including agricultural waste, e.g. corn stover (He et al. 2016) or palm-oil mill effluent (Rana et al. 2017), could be used to generate organic acids through cellulosic degradation (Ichikawa et al. 2018) aiding in breakdown of ore minerals (Lindsay et al. 1991) with further metal release promoted by DMRB e.g. *Geobacter* species (Lloyd. 2003).

2 Samples

There are two lateritic horizons of significant interest in terms of economic mineralization, the Lower Breccia (LB) and the Ferralite (FL). LB, (average thickness ~3m), is volumetrically subordinate to FL (average thickness ~12m), but hosts higher grades of Mn and Co (Fig. 1). Samples from both FL and LB horizons are used in this study in order to understand the differences in microbiomes vertically through the profile and their potential role in controlling trace metal solubility and mobility. Additional samples were selected from the upper limonite/ferruginous hardpan capping the laterite, a spoil heap and a highly Co- and Ni-enriched region of the southern trench.

3 Co-Ni Mineralogy

X-ray diffraction (XRD) was performed at the School of Earth and Environmental Sciences, University of Manchester, UK, in order to constrain mineralogy and mineralogical proportions and link to bulk-sample geochemical data obtained through X-ray Fluorescence. Lambiv-Dzemua et al. (2013) confirmed the presence of Co and Ni primarily in phyllomanganates, e.g. lithiophorite, asbolane and intermediates thereof.

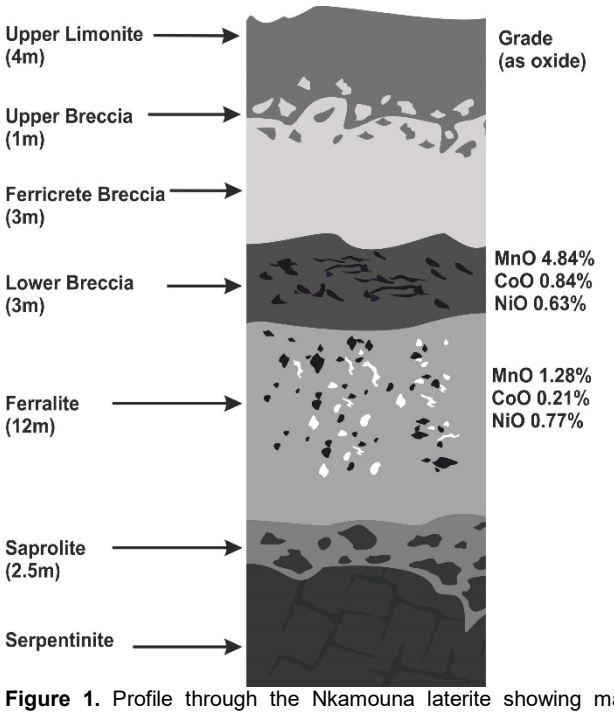

Figure 1. Profile through the Nkamouna laterite showing main horizons and thickness. Adapted from Lambiv-Dzemua et al. (2013).

Building on this work Co and Ni *K*-edge Extended X-ray Absorption Fine Structure (EXAFS) were performed at beamline I20, Diamond Light Source (DLS), UK, to fully constrain mineralogical sites. In lateritic environments Co is typically present as octahedrally coordinated ($_{Oh}$) Co^{3+} (Manceau et al. 1986), with an ionic radius (IR) of ~0.53Å, and has been previously demonstrated to be incorporated into the Mn-oxide sheet of phyllomanganates due to similarities in IR with $Mn^{3+}{}_{Oh}$ (~0.58Å) and $Mn^{4+}{}_{Oh}$ (~0.54Å) (Manceau et al. 2000). Ni, exhibiting significant differences in both IR (~0.69Å, $Ni^{2+}{}_{Oh}$) (Shannon. 1976) and valence, with respect to Mn^{3+}/Mn^{4+} occupies different sites dependent on a range of factors including height in profile and availability of mineral forming elements e.g. Mn and Al. These factors combined with redox conditions can either promote or inhibit incorporation of Ni into mineral phases.

Additional analyses performed on beamline 6.3.1 at the Advanced Light Source (ALS) synchrotron, Berkeley, CA, USA, allowed evaluation of valence and coordination of Mn in the ore through X-ray Absorption Spectroscopy (XAS) at the $L_{3,2}$-edge. Speciation of Mn in the ore, as the main constituent of the Co- and Ni-bearing oxide phases, has implications regarding the stability of these poorly defined minerals and therefore consequences in terms of phase-deconstruction and metal release during applied bio-processing methods.

4 Ore Incubation and Bio-Extraction

Samples were incubated in a synthetic groundwater with glucose as a carbon source and monitored at selected time-points for changes in fluid chemistry. Changes in Fe^{2+} (labile and aqueous), aqueous Fe, Mn, Co, Ni and Ba, and volatile fatty acids (VFAs) were measured by ferrozine assay, Inductively-Coupled Plasma Atomic-Emission Spectroscopy (ICP-AES) and Ion Chromatography, respectively. All samples showed Fe-reduction, release of Mn, Co, Ni and Ba, and generation of VFAs, e.g. formate, lactate and acetate, concomitant with reduction in pH. Differences in key geochemical parameters can be linked to a combination of factors including height in the laterite profile, mineralogy and geochemistry, which all affect the microbiome of each sampled region. Similarly, both rates of release and proportions of metals released can be linked to samples' vertical location as well as mineralogy and present considerations with respect to ore beneficiation especially where phases with high sorption capacity, e.g. Fe(III)-oxyhydroxides and clays, are abundant in the ore (Eylem et al. 1990; Ugwu et al. 2017).

5 Speciation of Bio-Extraction Products

Speciation of both Co and Mn in post-reduction aqueous phases was assessed through Co- and Mn *K*-edge X-ray Absorption Near Edge Structure (XANES), performed at beamline I20, DLS, UK. Results confirmed breakdown of Mn(III/IV)-oxides promoting release of Mn and Co to solution. Solid phase XANES analyses at the Mn and Ni K-edges were performed at beamline B18, DLS, UK and show both structural and speciation changes in the minerals with incubation. Supporting *L*-edge XAS results from 6.3.1, ALS, allowed characterisation of the solid phase, with respect to relative proportions of Mn^{4+}, Mn^{3+} and Mn^{2+}, with bulk reduction occurring relative to unstimulated ore. These techniques and their ability to define bioextraction products have underpinned this study.

6 Co-Ni-Asbolane Bioreduction

A poorly crystalline Co-Ni-asbolane, with high concentrations of Co and Ni, was synthesized by oxidative precipitation and characterized by XRD and Selected Area Electron Diffraction (SAED). Energy Dispersive X-ray Spectroscopy (EDS) and ICP-AES confirmed elemental proportions. XAS at the Mn-, Co- and Ni *L*-edges, performed at 6.3.1, ALS, allowed a tentative structure to be proposed based on speciation and coordination of Mn, Co and Ni.

The phase was suspended in bicarbonate buffer and reduced using a pure culture of *Geobacter sulfurreducens* using Na-acetate as electron donor. Dissolution and metal release was noted, consistent with the bioreduction mechanisms implied in the more complex sediment systems above.

7 Implications

Microbial consortia indigenous to Nkamouna ore offer an extraction method representing a way of integrating agro-industrial waste into the extraction of critical metals from lateritic ore and should offer cost-benefits by removing import and transport costs of elemental sulphur/sulphuric acid typically used in lateritic ore processing (Oxley et al.

2016). This will help offset the carbon footprint of reagent transport as well provide an extraction route with lower environmental risk. Gangue material from the ore, e.g. Fe-oxide rich waste, can be potentially repurposed for transformation into valuable by-products (Joshi et al. 2018).

Acknowledgements

This work has been done as part of the CoG3 project, funded as part of the NERC sponsored SoS Minerals project. Thanks are due to Richard Pattrick, without whom I would not be doing this project, Gideon Lambiv-Dzemua for assistance during sample collection, Paul Lythgoe and Al Bewsher (SEES, UK) for performing ICP-AES and IC analyses, John Waters and Heath Bagshaw (SEES, UK) for aid in mineralogical analyses, Alpha N'Diaye (ALS, USA) for aid in XAS experimental setup, Shusaku Hayama (DLS, UK) for aid in XANES/EXASF experimental setup, Laura Newsome (CSM, UK) for help throughout the main experiment, and Agustin Solano-Arguedas and Dawn Buchanan (SEES, UK) for help on numerous beamtimes.

References

BGS (2015) Risk List 2015 British Geological Survey - Commodity Statistics https://www.bgs.ac.uk/mineralsuk/statistics/riskList.html

Byrne JM, Coker VS, Wincott PL, Vaughan PL, Tuna F, Arenholz E, Van der Laan G, Pattrick RAD, Lloyd JR, Telling ND (2013) Controlled cobalt doping in biogenic magnetite nanoparticles. J R Soc Interface 10

de Haan, J, Geenen, S (2016) Mining cooperatives in Eastern DRC: The interplay between historical power relations and formal institutions. J Exis 3:823-831

Diemel JA (2018) Authority and access to the cassiterite and coltan trade in Bukama Territory (DRC). J Exis 5:56-65

European Commission (2017) Communication from the Commission of the European Parliament, the Council, the European Economic and Social Committee and the Committee of the Regions on the 2017 list of Critical Raw Materials for the EU. https://eur-lex.europa.eu/legal-content/EN/TXT/PDF/?uri=CELEX:52017DC0490&from=EN

Eylem C, Erten HN, Götürk H (1990) Sorption-desorption behaviour of barium on clays. J Environ Radioact 11 (2):183-200

He T, Jiang Z, Wu P, Yi J, Li J, Hu C (2016) Fractionation for further conversion of raw corn stover to lactic acid. Sci Rep 6:38623 1-11

Ichikawa S, Ichihara M, Ito T, Isozaki K, Kosugi A, Karita S (2018) Glucose production from cellulose through biological simultaneous enzyme production and saccharification using recombinant bacteria expressing the β-glucosidase gene. J Biosci Bioeng. In Press

Javadli R, de Klerk A (2012) Desulfurization of heavy oil. Appl Petrochem Res 1:3-19

Johannsen M, Gneckevow U, Eckelt L, Feussner A, Waldofner N, Scholz R, Deger S, Wust P Loening SA, Jordan A (2005) Clinical hyperthermia of prostate cancer using magnetic nanoparticles: Presentation of a new interstitial technique. Int J Hyperth 21:637-647

Joshi N, Filip J, Coker VS, Sadhukhan J, Safarik I, Bagshaw H, Lloyd JR (2018) Microbial reduction of natural Fe(III) minerals; toward the sustainable production of functional magnetic nanoparticles. Front Environ Sci 6:127.1-127.11

Kelly TD, Matos GR (2017) Historical statistics for mineral and material commodities in the United States (2017 version): USGS Data Series 140. https://minerals.usgs.gov/minerals/pubs/historical-statistics/

Joshi N, Filip J, Coker VS, Sadhukhan J, Safarik I, Bagshaw H, Lloyd JR (2018) Microbial reduction of natural Fe(III) minerals; toward the sustainable production of functional magnetic nanoparticles. Front Environ Sci 6:127.1-127.11

Lambiv-Dzemua G, Gleeson S, Schofield PF (2013) Mineralogical characterization of the Nkamouna Co–Mn laterite ore, southeast Cameroon. Min Dep 48:155-171

Lindsay WL (1991) Iron oxide solubilisation by organic matter and its effect on iron availability. Plant Soil 130: 27-34

Lloyd JR (2003) Microbial reduction of metals and radionuclides. FEMS Microbiol. Rev 27:411-425

Manceau A, Llorca S, Calas G (1986) Structural Chemistry of Mn, Co and Ni in some natural manganese-oxides. J Phys Colloques 47; C8-703-C8-707

Manceau A, Schliegel ML, Musso ML, Sole VA, Gauhtier C, Petit PE, Tolard F (2000) Crystal chemistry of trace elements in natural and synthetic goethite. Geochim Cosmochim Acta 64:3643-3661

Mouritz AP (Ed.) (2012) Introduction to aerospace materials. In: Introduction to aerospace materials: 1-14. Online: Woodhead Publishing

Mudd GM, Weng Z, Jowitt SM, Turnbull ID, Graedel TE (2013) Quantifying the recoverable resources of by-product metals: The case of cobalt. Ore Geol. Rev. 55:87-98

Nitta N, Wu F, Lee JT, Yushin G (2014) Li-ion battery materials: present and future. Mater Today 18 (5):252-264

Oxley A, Smith ME, Caceres O (2016) Why heap-leach nickel laterites? Min. Eng. 88:53-60

Perner A, Vetter J (2015) 8 – Lithium-ion batteries for hybrid electric vehicles and battery electric vehicles. In: SCROSATI B, GARCHE J, TILLMETZ W (Eds.) Advances in battery technologies for electric vehicles: 173-190. Online: Woodhead Publishing

Rana S, Singh L, Wahid Z, Liu H (2017) A recent overview of palm oil mill effluent management via bioreactor configurations. Curr Pollution Rep 3:254-267

Shannon RD (1976) Revised effective ionic radii and systematic studies of interatomic distances in halides and chalcogenides. Acta Cryst A32:751-767

Shedd KB (2018) USGS Mineral Commodity Surveys – Cobalt 2018. Available: https://minerals.usgs.gov/minerals/pubs/commodity/cobalt/mcs-2018-cobal.pdf

Shedd KB (2019) USGS Mineral Commodity Surveys – Cobalt 2019. Available: https://minerals.usgs.gov/minerals/pubs/commodity/cobalt/mcs-2019-cobal.pdf

Slack JF, Kimball BE, Shedd KB (2017) Cobalt. In: SCHULZ KJ, DEYOUNG JH, SEAL RR, BRADLEY DC (eds.). Critical mineral resources of the United States - economic and environmental geology and prospects for future supply. US Geological Survey Professional Paper 1802: F1-F40

Smith SL, Grail BM, Johnson BD (2016) Reductive bioprocessing of cobalt-bearing limonitic laterites. Min Eng 106: 86-90

Ugwu IM, Sherman DM (2017) Irreversibility of sorption of cobalt to goethite (α-FeOOH) and disparities in dissolution of aged synthetic Co-goethite. Chem Geol 467:168-176

United Nations (2015) World population prospects – Key findings and advance tables. https://esa.un.org/unpd/wpp/publications/files/key_findings_wpp_2015.pdf.

United Nations (2018) World urbanization prospects 2018. https://population.un.org/wup/Publications/

Sulphide trace element, sulphur isotope and hydrothermal alteration studies in the Juomasuo and Hangaslampi Au-Co deposits, Kuusamo belt, northeastern Finland

Mikael Vasilopoulos, Jukka-Pekka Ranta
University of Oulu, Finland

Ferenc Molnár, Hugh O´Brien, Yann Lahaye
Geological Survey of Finland, Espoo, Finland

Abstract. The Juomasuo and Hangaslampi Au-Co deposits are hosted by the Paleoproterozoic Kuusamo belt in northeastern Finland. Sulphur isotope and trace element data from sulphides indicate that the geochemically distinct, Au-Co and Co-only enrichments were formed from fluids of different origin. Accordingly, sericite alteration is typical in the zones of the Au-Co enrichment, whereas the chlorite-biotite-amphibole alteration occurs in relation to the Co-only mineralization. Variation in the composition of host rocks does not seem to have a strong control on the type of mineralization.

1 Introduction

Finland currently produces 66% of the EU cobalt supply, extracted from sulphide ores from the Sotkamo, Kevitsa, Hitura and Kylylahti mines (European Commission 2018). With the cobalt demand related to rechargeable batteries expected to rise in the following years, the importance of Finland's cobalt resources becomes even more pronounced. A better understanding of the formation processes of the already known Co-rich deposits is needed to enhance successes of exploration for new deposits.

This study concentrates on the Juomasuo and Hangaslampi Au-Co deposits, which are located in northeastern Finland, approximately 45 km north of the town of Kuusamo (Fig. 1). These deposits are situated in the Paleoproterozoic Kuusamo belt (KB) and are part of the Kuusamo-Kuolajärvi orogenic gold metallogenic area (Eilu et al. 2012), comprising several epigenetic Au-Co-Cu occurrences (Pankka 1992; Vanhanen 2001). Previous studies proposed different genetic classifications for the Au-Co-Cu mineralization including iron-oxide-copper-gold (IOCG), orogenic gold with atypical metal association, epithermal gold, Blackbird-type and syngenetic type (Pankka 1992; Vanhanen 2001; Eilu & Pankka 2009; Slack et al. 2012). The Juomasuo deposit is the most important known epigenetic-hydrothermal Au-Co deposit in the Kuusamo belt. Hangaslampi is situated approximately 1 km south from Juomasuo and is also mainly enriched in Au and Co. Cu, Mo and REE are the most typical associated trace metals in these deposits. For the purpose of better understanding the hydrothermal processes that led to

the mineralization in Juomasuo and Hangaslampi we applied *in situ* multi- and single collector LA-ICP-MS analytical techniques to study sulphur isotope and trace element characteristics of sulphide minerals from these deposits. Additionally, we utilized whole-rock geochemical data in order to classify the heavily altered host rocks and to study the control of the alteration mineralogy on the mineralization types with different metal associations at Juomasuo.

2 Regional geological setting

The KB is a part of the larger Karasjok-Kuusamo-Lake Onega belt that extends from northern Norway to the Lake Onega in Russia (Pankka 1992). The rocks comprising this belt are part of the Karelian supracrustal formations. Their age ranges from 2.5 to 1.9 Ga (Silvennoinen 1972, 1992). The KB was at least partially formed in an intracratonic failed rift setting related to the Paleoproterozoic breakup of the Archean Karelian craton (Hanski & Huhma 2005). The KB consists of several formations of volcanic and sedimentary origin,

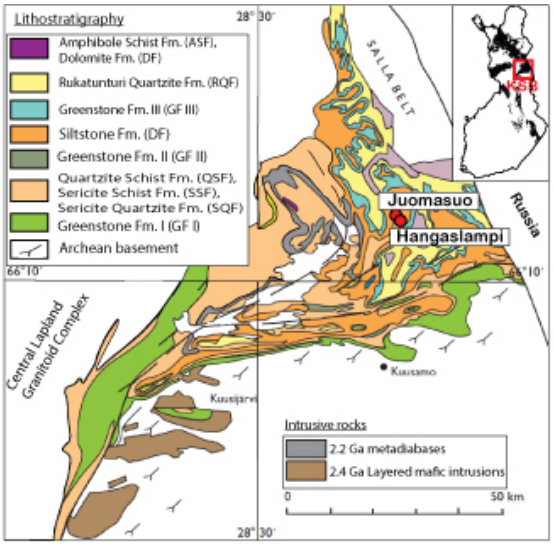

Figure 1. Simplified geological map of the Kuusamo belt. Modified after Laajoki (2015) and Vanhanen (2001).

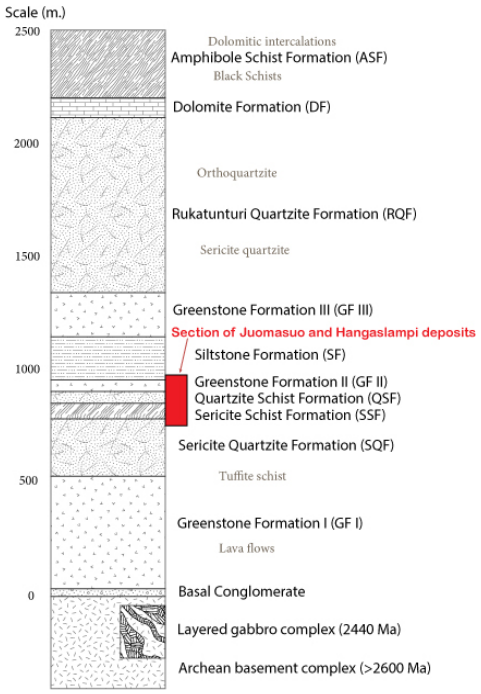

Figure 2. Stratigraphic column of the Kuusamo belt showing the location of Juomasuo and Hangaslampi in the stratigraphy. Modified after Silvennoinen (1972) and Vanhanen (2001).

including three or four stages of mafic volcanism with associated mafic sills and dykes (Pankka 1992). The stratigraphy of the Kuusamo belt was defined by Silvennoinen (1972) (Fig.2).

The stratigraphic sequence of the KB underwent deformation and regional metamorphism during the Svecofennian orogeny (1.9-1.8 Ga; Silvennoinen 1972, 1992). The metamorphic grades vary from lower greenschist facies in the central parts of the belt to upper amphibolite facies in the western parts, near the contact with the Central Lapland Granitoid Complex. Higher metamorphic grades are also present in the eastern part of the KB. Mineralization has been mostly encountered near the upper and lower boundaries of the Greenstone Formation II (GF II), but some mineralization is also hosted by the upper part of the Rukatunturi Quartzite Formation (RQF) (Vanhanen 1990, 2001) (Fig. 2).

3 Geology and mineralogy of the Juomasuo and Hangaslampi Au-Co deposits

The host rocks of the Juomasuo deposit are characterised by strong albitisation but the mineralised zones also contain quartz, chlorite, biotite, sericite, carbonate, amphibole and talc in addition to albite. The most abundant sulphide is pyrrhotite followed by pyrite and lesser chalcopyrite. Cobaltite can be found in the Co-rich parts of the ore as inclusions in pyrrhotite and sometimes in pyrite. Cobaltpentlandite is also present mainly as exsolutions in pyrrhotite. Molybdenite, rutile, magnetite, native Au and tellurides (altaite, tellurobismuthite and melonite) are noteworthy accessories in the deposit. The Juomasuo deposit consists of one major mineralized zone and several smaller adjacent sulphidized zones (Vanhanen 2001). The total mineral resource estimate for the Juomasuo deposit is 2.37 million tonnes grading at 4.6 g/t Au and 0.13 wt% Co and an additional 5.04 million tonnes of Co resources without Au grading at 0.12 wt% Co (Dragon Mining 2014).

The orebodies at Hangaslampi occur in a local antiform structure just below the GF II (Vanhanen 2001). The resource estimates amount to 403 thousand tonnes grading at 5.1 g/t Au and 0.06 wt% Co and an additional 180 thousand tonnes of ore grading at 0.1 wt% Co without Au (Dragon Mining 2014). The gangue minerals at Hangaslampi comprise albite, quartz, chlorite, biotite, sericite, lesser carbonate, amphibole and accessory tourmaline, apatite and zircon. The most common sulphide is pyrite. Pyrrhotite has a weak presence and is mostly found as inclusions in pyrite and magnetite and sometimes as disseminated grains in the silicates where it is occasionally associated with chalcopyrite. Cobaltite is rare in Hangaslampi and cobaltpentlandite occurs sporadically as exsolutions in the disseminated pyrrhotite. Magnetite is more widespread compared to Juomasuo. Other common accessory ore minerals at Hangaslampi include molybdenite and some minor tellurides.

4 Lithogeochemistry at the Juomasuo deposit

Previous studies have described the heavily altered and metamorphosed rocks at Juomasuo and Hangaslampi mainly on the basis of the dominating alteration minerals (Pankka 1992; Vanhanen 2001). For the Juomasuo deposit, the Dragon Mining Ltd. provided a detailed lithogeochemical dataset for the purpose of our studies and we utilized this database for the geochemical classification of the protoliths of the altered rocks. We combined drill core observations with immobile element ratios and recognized the following six rock types: ultramafic rock, mafic rock, intermediate rock, felsic rock, metasediment and albitite (Fig.3). By plotting the samples belonging to the Au-Co and Co-only type of ores on the Nb/Y-Zr/TiO_2 discrimination diagram, it is evident that both types of mineralization are present in all of the rock types, apart from the albitites and the ultramafic rocks (Fig. 3).

A second application of the lithogeochemical database was to calculate Molar Element Ratios (MER) to determine the control of the alteration mineralogy on the different types of mineralization. The MER diagrams (Fig. 4) show that different types of alteration affected different rock types. By plotting the gold and cobalt grades together with the MER data for the metavolcanic rocks it seems that gold enrichment is mainly associated with sericite alteration and much less with chlorite-biotite alteration (Fig. 4). Co enrichment is strongly associated with chlorite-biotite and amphibole alteration and additionally with sericite alteration (Fig. 4). Similar trends can be demonstrated for the metasediments.

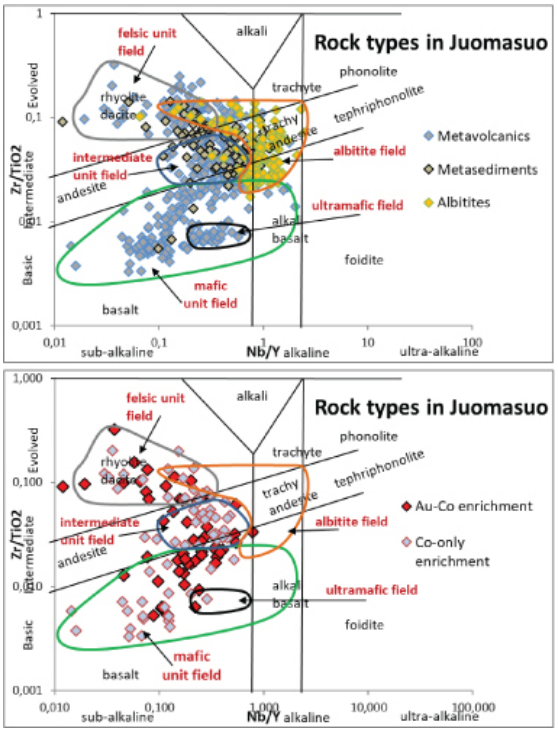

Figure 3. Fields for each rock unit recognized at Juomasuo on the Nb/Y-Zr/TiO_2 discrimination diagram (Pearce, 1996): Metasediments do not have a separate field as they are a mixture of both felsic and mafic components.

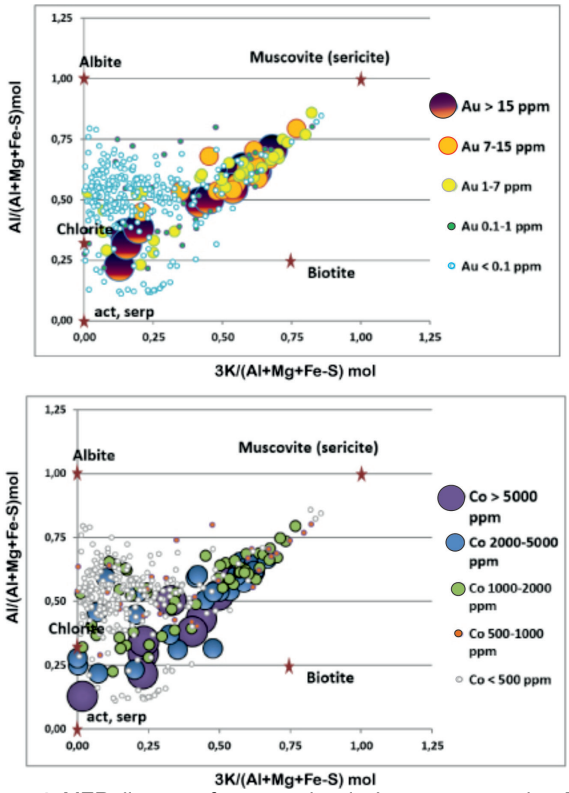

Figure 4. MER diagrams for metavolcanic Juomasuo samples. The selected molar elemental ratios of the axes represent well the alteration mineralogy of Juomasuo by allocating a specific position in the diagram to the most important alteration minerals.

5 Sulphur isotope and trace element data

Systematic sulphur isotope analyses were performed on pyrite, pyrrhotite and chalcopyrite from Juomasuo and Hangaslampi with the use of multi-collector LA-ICP-MS. Trace element contents of the same sulphide grains were determined by single-collector LA-ICP-MS analyses. Analytical spots for sulphur isotope and trace element determination were placed next to each other. Matrix-matched sulphide standards were used during these analyses.

Sulphides from the ore zones at Juomasuo have $\delta^{34}S$ values between -2.6 and +6.9 (median +3.45) and at Hangaslampi between -0.9 and +9 (median +5.3). Sulphides from barren samples range from -0.5 to +13.5. Whereas most of the values are positive, there is a shift to negative or near-zero values in some sulphides in both deposits (Fig. 5). By examining the Co/Ni ratio of pyrite grains from different mineralization types, distinct mineralization stages become evident: one represented by distinctly high Co/Ni ratios and one with low Co/Ni ratios. Pyrite grains with high Co/Ni ratios show a relatively narrow range of positive $\delta^{34}S$ values, whereas the grains with low Co/Ni ratios have a wider range of $\delta^{34}S$ values including all the negative ones (Fig. 5). A similar trend is present for the Se/S ratios of the two stages with the high Co/Ni pyrite having a narrow range of low Se/S ratio values and the low Co/Ni pyrite having

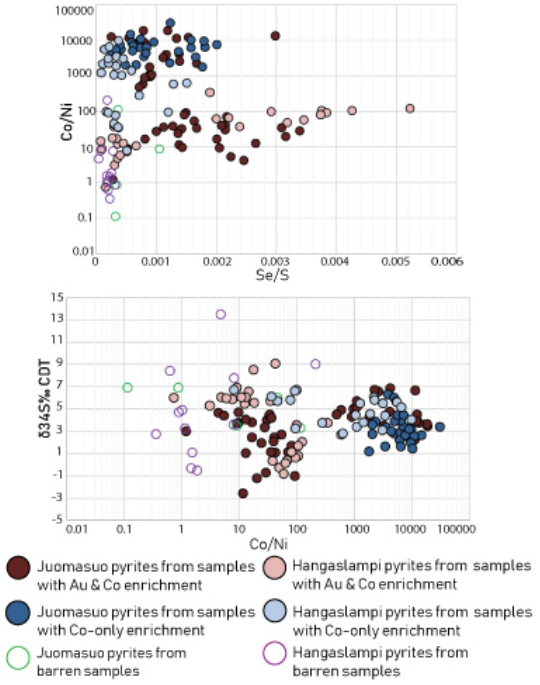

Figure 5. Results of sulphur isotope and trace element analyses on pyrite from Juomasuo and Hangaslampi.

a wider range. Other trace elements also vary systematically within the two Co/Ni ratio categories (Fig. 6). The Co/Ni ratio is mostly controlled by the Ni content of sulphides with differences up to two orders of magnitude (Fig. 6).

The wider range of $\delta^{34}S$, Se/S ratios and the relatively

high Ni, Se and Te contents in the low Co/Ni category could indicate a mixing of different fluid and sulphur sources. The low Co/Ni stage comprises mainly Au-Co mineralization in both deposits. The high Co/Ni category on the other hand has a narrow range of $\delta^{34}S$ and Se/S ratios and low Ni, Se and Te contents. The high Co/Ni stage could thus be attributed to a single hydrothermal event and a homogeneous sulphur source. The high Co/Ni stage mainly includes Co-only mineralization with some Au-Co mineralization included in Juomasuo.

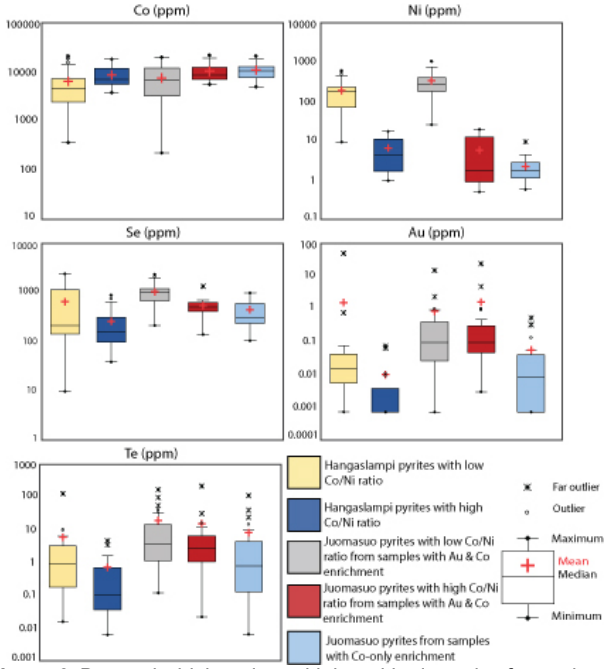

Figure 6. Box and whisker plots with logarithmic scales for analyzed pyrite from Juomasuo and Hangaslampi.

6 Summary and conclusions

The Juomasuo and Hangaslampi Au-Co deposits are characterized by multi-stage hydrothermal processes that are recorded in the sulphur isotope and trace element characteristics of sulphides. A hydrothermal stage responsible for the accumulation of the Co-only ores in both deposits, and some Au-Co mineralization in Juomasuo, deposited pyrite characterized by high Co/Ni ratios, low Se/S ratios and positive $\delta^{34}S$ values showing a relatively narrow range of values. Pyrite from a different stage of hydrothermal activity that created mostly Au-Co mineralization in both deposits is characterised by low Co/Ni ratios, a wide range of Se/S ratios, δ34S values and high Ni, Se and Te contents. The distinct sources of parent fluids are also supported by contrasting alteration parageneses of the same lithologies depending on enrichment type. The Au-Co mineralization in Juomasuo mainly occurs within sericite alteration zones whereas the Co-only mineralization is hosted by chlorite-biotite-amphibole alteration. These results are in agreement with the U-Pb dating of hydrothermal monazite from Hangaslampi suggesting two major stages of mineralization, one at 1.85 and the other at 1.81 Ga (Pohjolainen et al., 2017).

Acknowledgements

This work was supported by grants from the Vilho, Yrjö and Kalle Väisälä foundation, the K.H. Renlund foundation and by the Academy of Finland # 281670 – MinSysPro project.

References

Dragon Mining (2014) Asx announcement, 18 March 2014: Resource updates lift Kuusamo ounces. http://www.dragonmining.com/static/files/41/2014-03-18__resource_updates_lift_kuusamo_ounces.pdf Accessed 01 March 2019.

Eilu P, Korsakova M, Äikäs O (2012) F040 Kuusamo-Kuolajärvi Co-Au. In: Eilu, P (Ed.) Mineral deposits and metallogeny of Fennoscandia. Geological Survey of Finland, Special Paper 53: 306-310.

Eilu P & Pankka H (2009) FINGOLD – A public database on gold deposits in Finland. Version 1.0. Geological Survey of Finland. Digital data product 4.

European Commission (2018) Report on Raw Materials for Battery Applications (SWD (2018) 245/2 final) https://ec.europa.eu/transport/sites/transport/files/3rd-mobility-pack/swd20180245.pdf Accessed 02 March 2019

Hanski E & Huhma H (2005) Central Lapland greenstone belt. In: Lehtinen, M., Nurmi, P.A. & Ramo, O.T. (Eds.) Precambrian Geology of Finland – Key to the Evolution of the Fennoscandian Shield. Amsterdam, Elsevier: 139–194.

Laajoki K (2005) Chapter 7 Karelian supracrustal rocks in Lehtinen M, Nurmi PA, Rämö OT (ed.) Developments in Precambrian Geology. Elsevier, volume 14: 279-341.

Pankka H (1992) Geology and mineralogy of Au-Co-U deposits in the proterozoic Kuusamo volcansedimentary belt, northeastern Finland. A dissertation. Michigan Technological University, Geology.

Pearce JA (1996) A users guide to basalt discrimination diagrams. In: Wyman, D. A. (Eds.) Trace Element Geochemistry of Volcanic Rocks: Applications for Massive Sulphide Exploration. Geol. Assoc. Canada, Short Course Notes 12: 79-113.

Pohjolainen E, Molnár F, O´Brien H, Huhma H, Tiljander, M, Sorjonen-Ward P, Lukkari S, Johanson B (2017) U-Pb geochronology of monazite from the Hangaslampi gold deposit in the Paleoproterozoic Kuusamo schist belt, northern Finland: implications for dating multi-stage mineralizing events. Proceedings of the 14th SGA Biennial Meeting, vol. 3: 1039-1042.

Silvennoinen A (1972) On the stratigraphic and structural geology of the Rukatunturi area, northeastern Finland. Geological Survey of Finland, Bulletin 257.

Silvennoinen A (1992) General geological setting and deep fracture structures in the Kuusamo-Kuolajärvi-Paanajärvi area. In: Silvennoinen, A (ed.) Deep fractures in the Paanajärvi-Kuusamo-Kuolajärvi area. Proceedings of a Finnish-Soviet Symposium in Finland on September 18-21, 1989. Geological Survey of Finland, Special Paper 13: 5-10.

Slack JF (2012) Strata-bound Fe-Co-Cu-Au-Bi-Y-REE deposits of the Idaho Copper Belt: multistage hydrothermal mineralization in a magmatic-related iron oxide-copper-gold system. Economic Geology 107: 1089-1113.

Vanhanen, E (1990) Sulfidimalmi- ja kultatutkimukset Kuusamon ja Sallan kuntien alueilla vuosina 1983-1988 kohteissa Vilkaslampi, Painanteenniitty, Maitokoski, Perttuma-aapa, Juhonlampi, Pullealampi, Manalanniemi (In Finnish). Geological Survey of Finland, Unpublished report M19/4524/-90/2/10.

Vanhanen E (2001) Geology, mineralogy and geochemistry of the Fe-Co-Au-(U) deposits in the Paleoproterozoic Kuusamo Schists Belt, northeastern Finland. Geological Survey of Finland Bulletin 399.

Trace elements in Cu-(Fe)-S sulphides from inactive hydrothermal vent sites at TAG, Mid-Atlantic Ridge

Berit Lehrmann, Bramley J. Murton
National Oceanography Centre-Southampton, UK

Matthew J. Cooper, J. Andy Milton
School of Ocean and Earth Science, University of Southampton, UK

Abstract. Metals such as cobalt, tin, germanium, silver and selenium that are vital in high-technology applications and for transition to a low-carbon economy are frequently termed 'critical'. To determine whether seafloor massive sulphide (SMS) represent a potential future source of critical metals, copper minerals from hydrothermal mounds at different stage of development and age, located in the TAG area (Mid-Atlantic Ridge), were analysed by in-situ laser ablation inductively coupled plasma-mass spectrometry (LA-ICP-MS). The results show that critical metals reach concentrations up to several hundreds of ppm. However, the distribution of these elements is very heterogeneous even on the scale of a single sample suggesting. Future mining operation of SMS will target these deposit primary for base and precious metals with critical metals being extract as by-products.

1 Introduction

There is growing demand for a range of minerals required in green energy and high-tech applications. These are typically referred to a 'critical'. (Zepf et al 2014). Land-based mining activities are increasingly focusing on more remote and technically challenging environments (Carvalho 2017) that often result in a higher environmental impact. Seafloor massive sulphide deposits, which form through hydrothermal venting in today's oceans, may contribute to the resource of critical metals in the future (Hannington et al 2011). While recent estimates of the resource potential for base and precious metals of modern SMS are 600 Mt with a median grade of 3 wt.-% copper, 9 wt.-% zinc, 2 g/t gold and 100 g/t silver (Monecke et al 2016), the inventory of critical metals associated with SMS and their fate during alteration processes are poorly understood.

This paper presents insights into the trace element distribution in copper sulphide (chalcopyrite, idaite, chalcocite and covellite) minerals from different aged, inactive SMS sites from the TAG hydrothermal area at 26°09'N on the Mid-Atlantic Ridge (Fig. 1). Our in-situ LA-ICP-MS data show that the trace element budget of fresh chimney samples and weathered sulphide blocks differs by several orders of magnitude. In addition, a variation in trace elements between surface and sub-surface samples of the same mound can be observed. Such information is critical in the decision process for economically feasible exploitation strategies of SMS where critical metals will contribute to the overall resource as by-products..

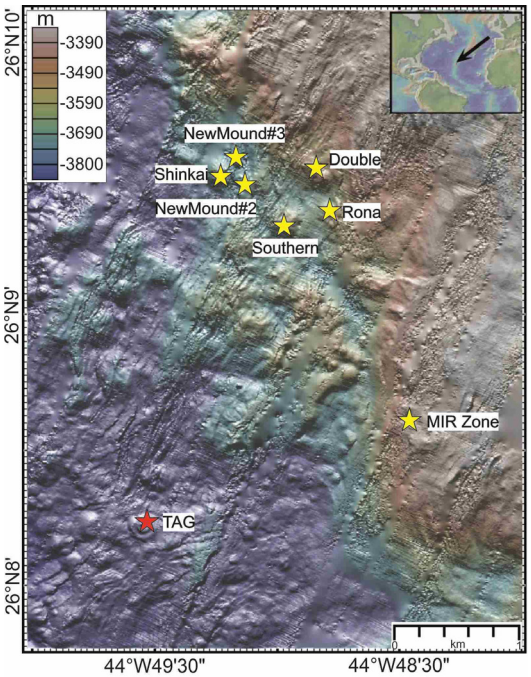

Figure 1. Bathymetric map (data source GeoMapApp: KN142-05 (TAG94), DSL120 2m grid White) of the TAG hydrothermal area and the location of the active and inactive hydrothermal sites studied in this project. The inset shows the locations on the Mid-Atlantic Ridge.

2 Geological Setting

The TAG hydrothermal area is one of the largest and best studied hydrothermal systems on earth (Rona et al 1986, 1993; Tivey et al 2003; Humphris et al 2015). Several active and relict hydrothermal sites, predominantly forming sulphide mounds are present in an area of 5x5 km. These mounds vary in size, stage of development and age. The active TAG mound, located in the southwest of the area, is currently in an active high-temperature stage, i.e. metal-rich black smoker fluids of ~365°Care discharged through multiple chimneys (Humphris et al 2015). North-northeast of the TAG mound several hydrothermal extinct mounds occur: Southern, Rona, Double, New Mound #2, New Mound #3 and Shinkai. Radiometric dating of sulphides from Double and Shinkai yield ages of 50 ka and 2-23 ka, respectively (Lalou et al 1995). Based on the proximity of New Mound #2 and #3 to Shinkai and Southern and Rona to Double it is assumed that these mounds are of similar development stages as the slope angles of the mounds, indicating the degree of anhydrite dissolution at depth, are very similar (Hannington et al 1998, Murton et al

2018).

3 Methodology

Thirteen copper-rich surface and subsurface samples, collected during expedition JC138 on *RRS James Cook* using a multipurpose robotic underwater vehicle and a robotic lander-type seafloor drill were investigated in this study. Samples were described macroscopically and studied under transmitted and reflected light to reveal their mineralogical composition.

Trace elements were analysed by LA-ICP-MS using a New Wave UP 193FX laser coupled to a Thermo Scientific XSeries 2 quadrupole ICP-MS at the University of Southampton. The ICP–MS operated with a plasma power of 1350 W, He (1 l/min) and N (0.01 l/min) were used as carrier gases while Ar acted as plasma (13 l/min) and auxiliary gas (0.8 l/min). Laser pulse frequency was set at 5 HZ and a laser energy density of 5-6 J/cm2 was chosen. The total analysis time for each spot was 45 s, including 20 s for gas blank analysis. A beam diameter of typically 25 µm and on occasion of 18 µm was used according to crystal size of the different copper sulphides.

In total 34 isotopes were monitored for quantitative analysis as well as mass positions of ^{77}ArCl and ^{83}Kr in order to quantify any interferences on ^{82}Se. NIST-610, NIST-612 (Jochum et al 2005) and MASS-1 (Wilson et al 2002) were used as external calibration standard. Analytical precision was monitored by the repeated analysis of the standards yielding <5% RSD for reported elements in this study on NIST610 (except Se 7.1 %) and <10% RSD on MASS-1. To monitor the instrument drift the sulphide standards were analysed for several times during an analytical day. After measurement the trace element concentrations were calculated with the PlasmaLab 2.6.1.335 software (Thermo Scientific) using Fe as internal standard determined by electron microprobe analysis on a Cameca-SX100 at the University of Edinburgh. Minimum detection limits were calculated following the protocol of Longerich et al 1996.

4 Results

4.1 Petrography

Massive sulphides recovered from the surface of Shinkai, New Mound #2 and #3 comprise chimneys and fragments of chimney material (Fig. 2A) whereas samples from Southern and Rona Mound comprise sulphide breccia and massive sulphide blocks (Fig. 2B). These samples are quite similar from drill core samples obtained from Southern, Rona and MIR Zone.

The interior of the chimney sample comprises an orifice of predominately chalcopyrite with an intercalated layer of idaite (Fig. 3A). Extending outwards, coarse-grained tetrahedral chalcopyrite is present that is altered to covellite along grain boundaries.

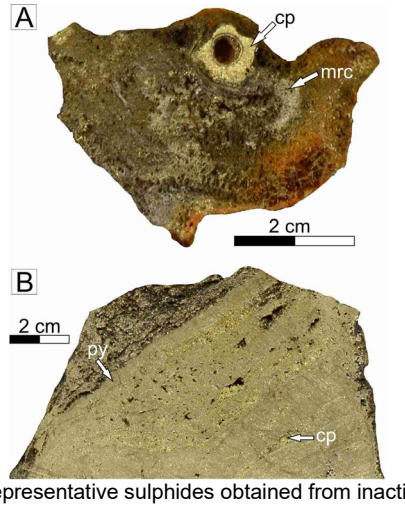

Figure 2. Representative sulphides obtained from inactive sulphide mounds from the TAG area. **(A)** Chimney with a chalcopyrite-rich orifice surrounded by marcasite; New Mound #2, 55-1A. **(B)** Massive sulphide talus comprising of pyrite with intercalated layers of chalcopyrite; Southern Mound, 21-3. Mineral abbreviations: cp: chalcopyrite, py: pyrite, mrc: marcasite.

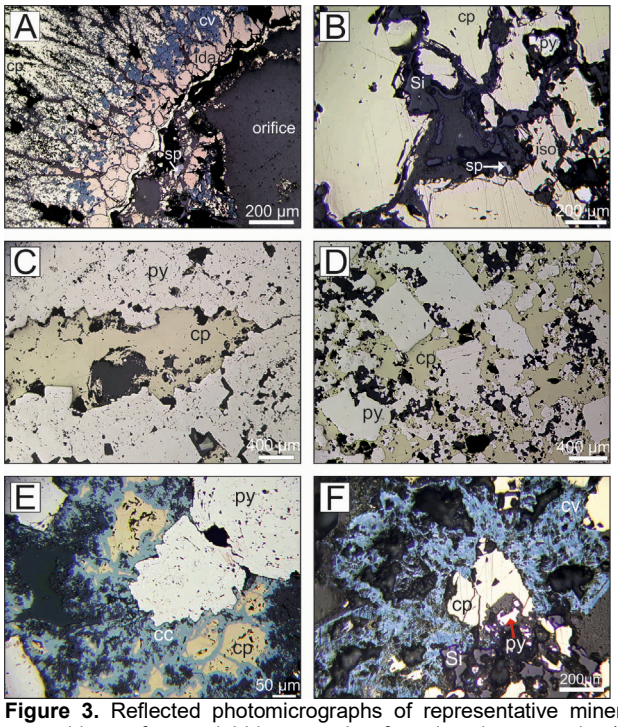

Figure 3. Reflected photomicrographs of representative mineral assemblages from sulphides samples from inactive mounds. (**A**) Cross-section of chimney comprising of tetrahedral shaped coarse-grained chalcopyrite, subhedral idaite altered to covellite along grain boundaries; New Mound #2, 55-1A. (**B**) Coarse-grained chalcopyrite with exsolution lamella of isocubanite and coated by a thin layer of amorphous silica; New Mound #3, 55-6A. (**C**) Massive recrystallized pyrite with intercalated layers of chalcopyrite; Southern Mound, 50-14. (**D**) Aggregates of pyrite surrounded by chalcopyrite; MIR Zone, 73-18. (**E**) Pyrite clasts surrounded by chalcopyrite that is altered to chalcocite along micro-fractures; Rona Mound, 45-7C. (**F**) Chalcopyrite surrounded by covellite with traces of amorphous silica and pyrite; New Mound #3, 55-6A. Mineral abbreviations: cp: chalcopyrite, iso: isocubanite/cubanite, ida: idaite, cc: chalcocite, cv: covellite, py: pyrite, sp: sphalerite, Si: amorphous silica.

Other chimney material from New Mound #3 comprises coarse-grained chalcopyrite that shows exsolution

lamella of isocubanite (Fig. 3B). Surface and subsurface samples from Southern, Rona and MIR Zone are formed of massive recrystallised pyrite that is intercalated with chalcopyrite layers (Fig. 3C) or coarse-grained cubic pyrite that is surrounded by massive chalcopyrite (Fig. 3D). Chalcopyrite is either altered to chalcocite along micro-fractures (Fig. 3E) or is surrounded by aggregates of fibrous covellite (Fig. 3F).

4.2 Trace element inventory of copper sulphides from different sites

Cobalt concentrations differ between chalcopyrite and other copper phases. While chimney material from New Mound #3 (55-6A) has on average cobalt content of 177±30 ppm (± 1σ), chalcopyrite from the chimney of New Mound #2 (55-1A) yields concentrations of 0.12±0.07 ppm cobalt (Fig. 4A). The chalcopyrite from the sub-surface samples at Southern and Rona yield an order of magnitude higher cobalt concentration, of 0.84±0.33 ppm and 3.28±3.62 ppm, respectively.

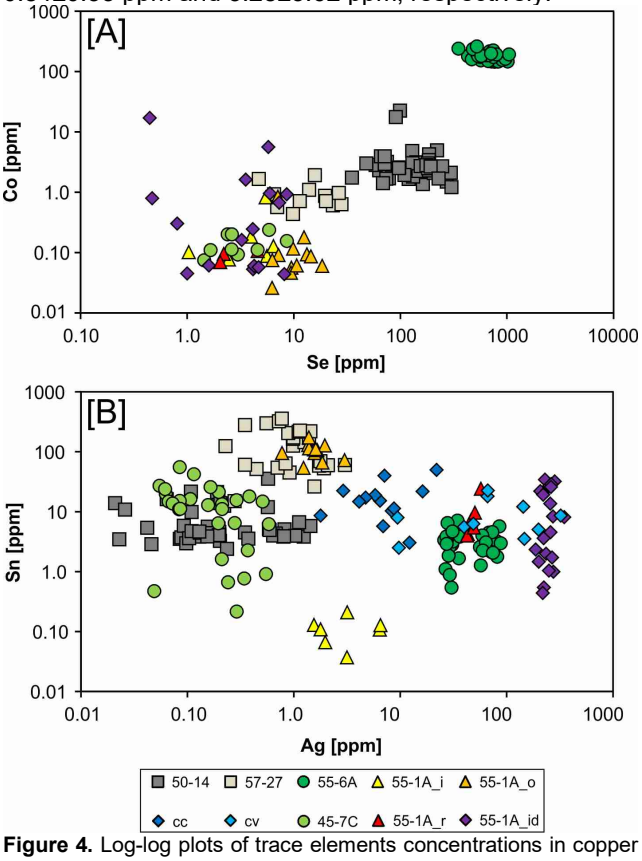

Figure 4. Log-log plots of trace elements concentrations in copper minerals from several inactive sulphide mounds at the TAG area. (**A**) Cobalt (Co) versus Selenium (Se) and (**B**) Tin (Sn) versus silver (Ag). Chimney 55-6A and 55-1A differ with regards to their trace element concentration, while sub-surface samples 50-14 and 57-27 show similar trace element pattern. Copper phases other than chalcopyrite can be quite enriched in silver.

A similar pattern can be observed for selenium concentrations. Again the chimney (55-6A) yields the highest concentration of 679±152 ppm Se, the other chimney (55-1A) shows average concentrations between 4.17±1.9 and 10.4±3.6 ppm. Again the sub-surface samples have intermediate selenium concentrations.

Tin concentrations are very similar in the majority of samples and copper phases (Fig. 4B). One sub-surface sample (57-27) and one generation of chalcopyrite from a chimney (55-1A) yield very high tin concentrations of 140±97 ppm and 104±30 ppm, respectively. In contrast chalcopyrite from the inner conduit of 55-1A shows the lowest tin concentrations (0.11±0.05 ppm).

Silver is predominately enriched in idaite, chalcocite and covellite rather than in chalcopyrite with the highest concentration being detected in idaite (246±35 ppm). The only exception is chalcopyrite from the other chimney (55-6A) where a concentration range between 26-89 ppm is observed.

Other elements such as gallium, germanium, indium and bismuth also show elevated concentrations of up to several hundreds of ppm in some samples and copper phases.

4.3 Trace element concentrations in one chimney sample

Trace element distribution is not only heterogeneous on a mound scale but also varies within a single sample. This can be observed in different chalcopyrite generations and idaite from chimney 55-1A (Fig. 5). While silver and cobalt yield the highest concentrations in the idaite, selenium and tin are enriched in the chalcopyrite of zone two. Chalcopyrite from the inner layer (zone 4) has elevated concentrations of germanium (287±136 ppm).

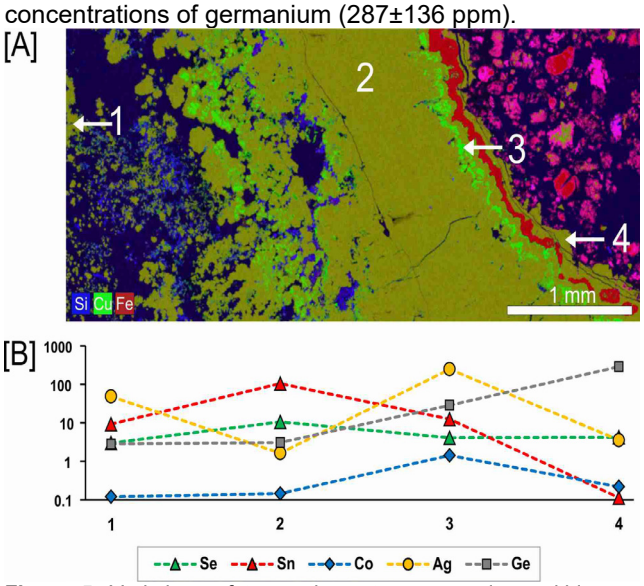

Figure 5. Variations of trace element concentrations within one chimney samples from New Mound #2. (**A**) Scanning electron microprobe map illustrating the major element distribution on the scale of several mm. Zone 1 is coarse grained chalcopyrite (referred to as 55-1A_r in figure 4), zone 2 is massive chalcopyrite forming the outer layer of the orifice (55-1A_o), zone 3 comprises idaite and zone 4 is chalcopyrite that forms the inner layer of the orifice (55-1A_i). (B) Log-line plot showing the change of concentrations across the four zones. Concentrations plotted are the mean values.

5 Conclusions

Bulk geochemical data for fresh chimney samples and sub-surface drill core from the literature suggest that

chimney samples from SMS deposits have the highest variety and concentrations of trace elements (Monecke et al 2016). However, in-situ LA-ICP-MS data provides further insight. Certain chimneys are enriched in high-temperature trace elements such as selenium and tin (Maslennikov et al 2009). Notably, some recrystallised chalcopyrite from subsurface samples can also exhibit this trace element signature whereas other sub-surface samples as well as surface material do not appear to host any significant quantities of trace elements. Secondary copper minerals can incorporate high concentrations of silver but do acquire many other trace elements.

In summary, our data show that copper phases can host critical metals at concentrations of up to several orders of magnitude, but their distribution is highly variable even at the scale of individual samples.

Acknowledgements

We thank the officers and crew of the *RRS James Cook*, and the shipboard technical and scientific party for their constant help and support throughout expedition JC138. Thanks to Duncan Muir from Cardiff University (SEM-time) and Chris Hayward from University of Edinburgh (EMPA-time). This work was funded by the European Union Seventh Framework Program (EU-FP7) "Blue Mining: breakthrough solutions for the sustainable deep-sea mining value chain" under grant No. 604500.

References

Carvalho FP (2017) Mining industry and sustainable development: time for change. Food and Energy Secur. 6:61-77. doi: 10.1002/fes3.109

Hannington MD, De Ronde CEJ, Petersen S (2005) Sea-Floor Tectonics and Submarine Hydrothermal Systems. In: Hedenquist JW, Thompson JFH, Goldfarb RJ, Richards JP (eds) Economic Geology One Hundredth Anniversary Volume, Soc. Econ. Geol., Littleton, pp 111–141

Hannington M, Jamieson J, Monecke T, Petersen S, Beaulieu S (2011) The abundance of seafloor massive sulphide deposits. Geol. 39:1155–1158. doi:10.1130/G32468.1

Humphris SE, Tivey MK, Tivey MA (2015) The Trans-Atlantic Geotraverse hydrothermal field: A hydrothermal system on an active detachment fault. Deep Sea Res. Part II 121:8–16. doi:10.1016/j.dsr2.2015.02.015

Jochum KP, Herwig K, Lammel E, Stolland B, Hofmann AW (2005) GeoReM: A New Geochemical Database for Reference Materials and Isotopic Standards. Geostand. Geoanalytical Res. 29:333-338. doi.org/10.1111/j.1751-908X.2005.tb00904.x

Lalou C, Reyss JL, Brichet E, Rona PA, Thompson G (1995) Hydrothermal activity on a 105-year scale at a slow-spreading ridge, TAG hydrothermal field, Mid-Atlantic Ridge 26°N. J. Geophys. Res.: 100 17855–17862. doi:10.1029/95JB01858

Longerich HP, Jackson SE, Günther D (1996) Laser Ablation Inductively coupled plasma mass spectrometric transient signal data acquisition and analyte concentration calculation. J. Anal. At. Spectrom. 11: 899-904. 10.1039/JA9961100899

Maslennikov VV, Maslennikova SP, Large RR, Danyushevsky LV (2009) Study of Trace Element Zonation in Vent Chimneys from the Silurian Yaman-Kasy Volcanic-Hosted Massive Sulfide Deposit (Southern Urals, Russia) Using Laser Ablation-Inductively Coupled Plasma Mass Spectrometry (LA-ICPMS). Econ. Geol. 104: 111-1141. 10.2113/gsecongeo.104.8.1111

Monecke T, Petersen S, Hannington MD, Grant H, Samson IM (2016) The minor element endowment of modern seafloor massive sulphides and comparison with deposits hosted in ancient volcanic successions. In: Verplanck PL, Hitzman MW (eds.) Rare Earth and Critical Elements in Ore Deposits, Soc. Econ. Geol, Knoxville, pp. 245–306.

Murton BJ, Shipboard Scientific Party (2018) Cruise Report: Expedition JC 138: 29th June–8th August 2016, Mid Atlantic Ridge, 26° 8.38′N, 44° 49.92′W. National Oceanography Centre Southampton. https://www.bodc.ac.uk/resources/inventories/cruise_inventory/reports/jc138.pdf. Accessed 01 March 2019

Rona PA, Klinkhammer G, Nelsen TA, Trefry JH, Elderfield H (1986) Black smokers, massive sulfides, and vent biota at the Mid-Atlantic Ridge. Nat. 321: 33–37. doi:10.1038/321033a0

Rona PA, Bogdanov YA, Gurvich EG, Rimski-Korsakov A, Sagalevitch AM, Hannington MD, Thompson G (1993) Relict hydrothermal zones in the TAG hydrothermal field, Mid-Atlantic Ridge 26°N, 45°W. J. Geophys. Res. 98:9715–9730. doi:10.1029/93JB00552

Tivey MA, Schouten K, Kleinrock MC (2003) A near-bottom magnetic survey of the Mid-Atlantic Ridge axis at 26°N: Implications for the tectonic evolution of the TAG segment. J. Geophys. Res. 108:2277–2789. doi:10.1029/2002JB001967

Wilson SA, Ridley WI, Koenig AE (2002) Development of sulfide calibration standards for the laser ablation inductively-coupled plasma mass spectrometry technique. J. Anal. At. Spectrom. 17:406-409. doi: 10.1039/b108787h

Zepf V, Reller A, Rennie C, Ashfield M, Simmons J, BP (2014). Materials critical to the energy industry: an introduction. https://www.bp.com/content/dam/bp/pdf/sustainability/group-reports/ESC_Materials_handbook_BP_Apr2014.pdf. Accessed 15 June 2016